10-1-2019

Characterizing three types of negative narrow bipolar events in thunderstorms

Sampath Bandara
University of Mississippi

Thomas Marshall
University of Mississippi

Sumedhe Karunarathne
University of Mississippi

Nilmini Karunarathne
University of Mississippi

Raymond Siedlecki
University of Mississippi

See next page for additional authors

Recommended Citation

Bandara, S., Marshall, T., Karunarathne, S., Karunarathne, N., Siedlecki, R., & Stolzenburg, M. (2019). Characterizing three types of negative narrow bipolar events in thunderstorms. Atmospheric Research, 227, 263–279. https://doi.org/10.1016/j.atmosres.2019.05.013

Atmospheric Research 227 (2019) 263–279

Contents lists available at ScienceDirect

Atmospheric Research

journal homepage: www.elsevier.com/locate/atmosres

Characterizing three types of negative narrow bipolar events in thunderstorms

Sampath Bandara, Thomas Marshall*, Sumedhe Karunarathne[1], Nilmini Karunarathne, Raymond Siedlecki, Maribeth Stolzenburg

Department of Physics & Astronomy, University of Mississippi, University, MS 38677, USA

ARTICLE INFO

Keywords:
Narrow bipolar event
Lightning
Lightning initiation
Initial breakdown pulses

ABSTRACT

Data from fast antennas (FAs) with bandwidth of 16 Hz–2.5 MHz and VHF power sensors (Log-RF) with bandwidth of 186–192 MHz are used to examine negative narrow bipolar events, or NNBEs. The main focus is on low-altitude (< 8.0 km) NNBEs that initiate negative cloud-to-ground (-CG) flashes; very few low-altitude NNBEs have been studied previously. For comparison, 24 high-altitude (> 8.0 km) NNBEs are also examined. The low-altitude NNBEs are found to have two types called NNBE(L) and NNBE(H). NNBE(L)s have a bipolar FA waveform typical of NBEs while NNBE(H)s have a unipolar FA waveform. It is hypothesized that NNBE(H)s may be weak versions of NNBE(L)s in which the second, overshoot part of the bipolar waveform is too weak to detect amid the FA sensor noise. Together the 33 NNBE(L)s and NNBE(H)s occurred at an average altitude of 6.2 km (range 4.6–7.8 km), had average range-normalized (to 100 km) amplitude of 0.4 V/m (range 0.06–1.5 V/m), and had average VHF power of 130 W (range 1–1300 W). These low-altitude NNBE properties are substantially smaller and weaker than the same properties of the high-altitude NNBEs and of positive NBEs that initiate intracloud (IC) flashes; these analyses indicate that -CG flashes are easier to initiate than IC flashes. Visual inspection of the FA and Log-RF data of 868 -CG flashes showed that only 33 flashes (4%) were preceded by either an NNBE(L) or NNBE(H), so 96% of the -CG flashes investigated probably did not begin with an NNBE.

1. Introduction

Narrow bipolar events (NBEs) are a type of electrical discharge associated with thunderclouds (e.g., Karunarathne et al., 2015). (NBEs are also known as narrow bipolar pulses, or NBPs, and as compact intracloud discharges, or CIDs.) Le Vine (1980) first identified NBEs and stated, based on measurements using the HF and VHF radio bands, that NBEs were "the sources of the strongest RF radiation during lightning." With an electric field change sensor (called an "E-change" sensor or "fast antenna" herein) with a bandwidth of 500 Hz–2 MHz, Le Vine (1980) found that an NBE produced a bipolar pulse with a short duration (10 − 20 μs). Le Vine (1980) described the bipolar NBE as having "an initial negative half cycle followed by a positive overshoot"; we will use "initial half cycle" and "overshoot" to describe the two opposite polarity parts of the NBE bipolar pulse. NBEs were originally thought to be temporally isolated from other lightning discharges (e.g., Willett et al., 1989; Smith et al., 1999), but Rison et al. (1999) showed that some NBEs initiate intracloud (IC) flashes, and Karunarathne et al. (2015) found that among 226 NBEs, only 37% occurred with no other lightning event within 10 km and 660 ms. Using the physics definition of electric field polarity, Willett et al. (1989) noted that NBEs can be either positive or negative based on the polarity of the initial deflection of the bipolar electric field change pulse. Azlinda Ahmad et al. (2010) compared the characteristics of positive and negative NBEs detected in Malaysia. Herein we focus on negative NBEs (NNBEs).

Smith et al. (2004) located > 100,000 positive and negative NBEs in the USA and found that the majority of positive NBEs occurred at altitudes of 7–15 km and the majority of NNBEs occurred at altitudes of 15–20 km, but small numbers of both types of NBEs were located down to an altitude of 4 km. Wu et al. (2012) studied the altitudes of > 8000 NBEs in China and found that most NNBEs occurred between 16 and 19 km altitude while most positive NBEs occurred between 8 and 16 km, though the minimum altitudes of NNBEs and positive NBEs were 7.0 and 6.4 km, respectively. Liu et al. (2018), using satellite and ground based sensors, reported that some high altitude NNBEs that occurred near cloud top initiated blue discharges such as blue jets or blue starters (e.g., Wescott et al., 1995). Wu et al. (2011) determined that their NNBEs (all 174 of which were located at altitudes of

* Corresponding author.
E-mail address: marshall@olemiss.edu (T. Marshall).
[1] Present address: Baptist College of Health Sciences, Memphis, TN 38104, USA.

https://doi.org/10.1016/j.atmosres.2019.05.013
Received 31 January 2019; Received in revised form 13 April 2019; Accepted 13 May 2019
Available online 15 May 2019

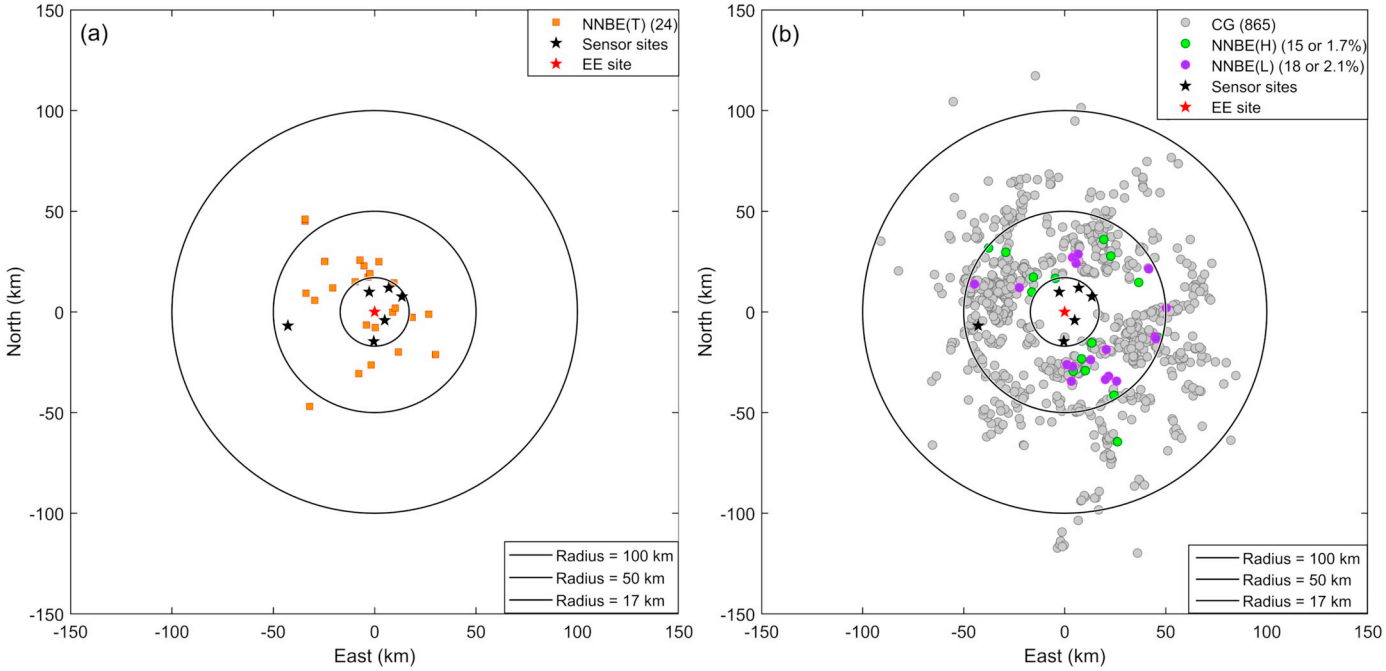

Fig. 1. (a) Plan view of seven sensor sites (marked with stars) along with locations of 24 NNBE(T)s (orange squares). The central sensor site, EE, is marked with the red star and is the origin of the coordinate system; three range rings are also shown. (b) Plan view of seven sensor sites along with locations of the first return stroke of 868 -CG flashes with locatable IB pulses. Of these 868 -CG flashes, 833 were not preceded by an NNBE (gray circles), 18 were preceded by NNBE(L)s (purple circles), and 15 were preceded by NNBE(H)s (green circles). (For interpretation of the references to color in this figure legend, the reader is referred to the web version of this article.)

15–20 km) had on average larger range-normalized E-change amplitudes than 555 positive NBEs, with the ratio of their respective geometric mean values being 1.4. We refer to these high altitude NNBEs as typical NNBEs or NNBE(T).

Using an HF/VHF (20–80 MHz) digital interferometer, a VHF Lightning Mapping Array (LMA), and a fast antenna, Rison et al. (2016) reported that positive NBEs initiate most or all IC flashes and that NNBEs initiate most or all negative cloud-to-ground (-CG) flashes. The mechanism for NBEs was determined to be "fast positive breakdown." Since -CG flash initiations typically occur below 7 km altitude, the initiating NNBEs represent a previously unknown group of low altitude NNBEs. For NBEs detected with the interferometer, Rison et al. (2016) found that the positive NBEs initiating IC flashes had VHF powers in the range 0–53.5 dBW while the NNBEs initiating -CG flashes were much weaker, 2 to 28 dBW. In addition, the waveforms of the NNBEs initiating -CG flashes had a "more monopolar" electric field change rather than the usual bipolar waveform; i.e., the NBE overshoot was missing or was very small (see Fig. 4c and d, Rison et al., 2016). We refer to this type of NNBE as "hump-like" or NNBE(H).

Marshall et al. (2014) and Chapman et al. (2017) showed that most or all -CG flashes and intracloud (IC) flashes begin with an impulsive initiating event, followed by an initial E-change (or IEC) that may include one or more short-duration low-amplitude initial breakdown (IB) pulses, followed by the first classic IB pulse (or "1stCIBP"). (A "classic" IB pulse is defined herein as having a bipolar waveform, a duration ≥10 μs, and a relatively large amplitude; classic IB pulses often have one or more "subpulses" on the initial half cycle of the bipolar waveform (Weidman and Krider, 1979). We note that this definition of classic IB pulse is not based on a particular physical mechanism, so the 10 μs minimum duration is somewhat arbitrary.) As shown by Rison et al. (2016), the impulsive initiating event may sometimes be an NBE. However, Marshall et al. (2019) found that one -CG and two IC flashes began without a fast antenna pulse. Since a bipolar fast antenna pulse is the hallmark of an NBE, one conclusion of Marshall et al. (2019) was that some -CG and IC flashes are initiated without an NBE. Marshall et al. (2019) also found that there was a short-duration (~1 μs), low-power (< 1 W, or < 0 dBW) VHF event initiating each of these flashes. Lyu et al. (2019) used a wideband digital interferometer (20–55 MHz) to study lightning initiation in IC flashes. For 26 flashes within 10 km of the interferometer, Lyu et al. (2019) reported two types of initiation events: (i) fast positive breakdown/NBE (12% of 26 flashes) and (ii) a series of "several to several tens of short VHF pulses with time scale of typically less than 0.5 μs" (88% of 26 flashes). Thus the findings of Lyu et al. (2019) support the two types of initiation events found in Rison et al. (2016) and Marshall et al. (2019).

Herein we report on NNBEs using an array of fast antennas and VHF power detectors. After determining their waveform shape and altitude, we divided the NNBEs into three groups (including the two types described above): (1) typical, high-altitude NNBE(T)s, (2) low-altitude, hump-like NNBE(H)s, and (3) low-altitude NNBEs with normal bipolar waveforms that we call NNBE(L)s. The NNBE(L)s are previously unreported. The two main goals of this study are to show data that indicate NNBE(H)s and NNBE(L)s initiate some but not all -CG flashes, and to characterize the properties of NNBE(H)s and NNBE(L)s, including range-normalized *E*-change amplitude and VHF power.

2. Data and analysis methods

2.1. Instrumentation

NNBE data for this study were collected during July and August 2016 using a seven-site array of lightning sensors located in and around Oxford, Mississippi, USA. Detailed description of the lightning sensor array can be found in Marshall et al. (2019). In brief, the array consisted of 6 inner sites (identified as EE, FS, IH, JM, SS, TM) located within 17 km of the EE site (which serves as the origin of our coordinate system), plus a seventh site (identified as NDS) located 43 km WSW of the EE site. Fig. 1a shows the plan position of the seven sensor sites denoted by stars, with a red star at the EE site. (Fig. 1a also shows data that are discussed later). Each site in the array was equipped with four

sensors: E-change Fast antenna or "FA" (10 *ms* decay time, bandwidth 16 *Hz* – 2.6 MHz), E-change Slow antenna or "SA" (1.0 s decay time, bandwidth 0.16 *Hz* – 2.6 MHz), electric field time derivative sensor or "*dE/dt*" (bandwidth 0 – 2.5 MHz), and VHF antenna or "Log-RF" (a logarithmic power sensor with a bandwidth 186–192 MHz). At each site all four sensors were triggered by the FA whenever a floating threshold was exceeded by an E-change pulse. For each trigger a 400 ms data record with 250 ms of pre-trigger and 150 ms of post-trigger was stored for each of the four sensors; these data were time stamped using Global Positioning System (GPS) pulse-per-second output (with a 1 sigma average < 2 ns). Lightning data captured by each antenna were digitized with a 10 MS/s, 12-bit digitizer. For each trigger, the data from FA, SA, *dE/dt*, and Log-RF antennas were recorded at sample rates of 5 MS/s, 5 MS/s, 10 MS/s, and 10 MS/s, respectively. Any new fast antenna trigger during the post-trigger period would extend the post-trigger period by 150 μs from the time of the new trigger.

2.2. Determining NNBE locations

Fast antenna data from the seven-station array can be used to locate the position (t, x, y, z) of fast pulse events using the time-of-arrival (TOA) method described in Karunarathne et al. (2013). This method, called PBFA (for "position by fast antenna"), requires usable FA data from at least 5 sites to find pulse locations. A Monte Carlo technique was used to estimate the errors in t, x, y, and z (see Karunarathne et al., 2013). In this study we sometimes used PBFA for NNBE locations whenever 5 or more sites had FA data with reasonable signal to noise. PBFA was also used sometimes to locate other fast antenna pulses, such as initial breakdown pulses and return strokes. As will be seen, the locations of initial breakdown pulses (also called IB pulses or IBPs) provide context for the locations of the NNBE(L)s and NNBE(H)s that initiate -CG flashes.

The dE/dt sensors also allow us to locate NNBEs and the other fast pulses just mentioned. The dE/dt sensors are especially useful for locating IB pulses that have small amplitudes in the FA data. The dE/dt data at each sensor site can be numerically integrated to produce fast-antenna-like waveforms (e.g., Jerauld et al., 2008). Thus, NNBEs and other lightning pulses can be located with $\int dE/dt$ waveforms from at least 5 sensor sites using the PBFA TOA algorithm; these locations are labeled as "$\int dE/dt$." Herein most of the locations of NNBEs and other lightning pulses were determined using $\int dE/dt$.

2.3. Calculating NNBE range-normalized amplitudes and NNBE VHF source powers

Locating the NNBEs is especially important since the locations allow us to compare our measurements with previously published data of NNBEs and of positive NBEs. For instance, a typical way of quantifying NNBE amplitudes in the FA data is to range-normalize them to 100 km using a 1/R dependence, where R is the slant range from the NNBE to the FA sensor. This range dependence assumes that the NNBE E-change amplitude is dominated by "radiation" component with essentially no "induction" or "electrostatic" contributions (see Uman et al. (1975) for the definition of these terms). Herein, the words "range-normalized" will imply that the range chosen was 100 km; we also use "E_{100km}" to indicate the range-normalized amplitude of FA pulses. The E_{100km} value of NNBEs was determined by averaging the range-normalized data from all FA sensors with range > 20 km.

A typical way to quantify NBE amplitudes in the HF and VHF radio bands is to calculate the NBE source power, P_S, in watts or dBW using the Friis transmission equation (e.g., Balanis, 2005):

$$P_S = \frac{P_r}{G_S G_r \left(\frac{\lambda}{4\pi R}\right)^2 |\hat{n}_S \bullet \hat{n}_r^*|^2} \quad (1)$$

where P_r is the power received by the Log-RF antenna, G_S and G_r are the gains of the emitting and receiving antennas (here, the NNBE and the Log-RF antenna, respectively), R is the slant range between the NNBE and the Log-RF antenna, λ is the wavelength of the VHF radiation (~1.6 m for the center frequency of 189 MHz), $\hat{n}_s$ is the unit polarization vector of the VHF radiation, and $\hat{n}_r$ is the unit polarization vector of the Log-RF antenna.

Below we calculate the source power, P_S, of NNBEs using Eq. (1) and express the power in watts (and sometimes in dBW, decibels relative to 1 watt). The antenna gains G_S and G_A are taken to be unity. R is known from PBFA or $\int dE/dt$ locations of the NNBEs. The expression $|\hat{n}_S \bullet \hat{n}_r^*|^2$ is the polarization loss factor (PLF) and can vary from 0 to 1 (Stutzman and Thiele, 2013). The PLF for reception of a linearly polarized wave with a linearly polarized receiving antenna is

$$|\hat{n}_S \bullet \hat{n}_r^*|^2 = |\cos\theta|^2 \quad (2)$$

The Log-RF receiving antenna was vertically polarized. We assume that the VHF radiation of an NNBE was isotropically emitted and was due to vertical charge motions, so it was vertically polarized. From the receiving antenna, θ was the angle measured upward from the horizontal to the NNBE; at long range θ was approximately 0 rad, so the PLF has been assumed to be 1.0. Thus, in using Eq. (1) for determining Log-RF power, we set G_S, G_r, and $|\hat{n}_S \bullet \hat{n}_r^*|$ equal to one. However, later we consider the possibility that the NNBE charge motions might not always be vertical, meaning that $|\hat{n}_S \bullet \hat{n}_r^*|$ would be < 1.

2.4. Identification of typical NNBEs

Although our main goal was to investigate the NNBEs that initiate -CG flashes, we first identified typical NNBEs or NNBE(T)s in our dataset for comparison. Le Vine (1980) showed that NBEs have especially strong VHF powers; we used this fact in a search algorithm to find NNBE(T)s. We programmatically searched each 400 ms record of triggered data obtained at the EE station for Log-RF pulses having peak amplitude greater than a threshold, which we adjusted to find only the largest Log-RF pulses. To find only negative NBEs, the program required that the initial polarity of the coincident fast antenna waveform was negative. In addition, we required that the candidate NNBE(T)s had triggered data at five or more sensor sites so that we could use either PBFA or $\int dE/dt$ to locate NNBE(T)s. Then, for each candidate NNBE(T) found in the Log-RF data, we visually examined the coincident fast antenna data of to ensure that each candidate had a typical bipolar NBE waveform with a duration < 50 μs. This procedure produced 174 NNBE (T)s. For further analysis, we then focused only on NNBE(T)s with horizontal location errors Δx and Δy < 2 km and chi squared goodness-of-fit values < 5, leaving a set of 24 NNBE(T)s.

These 24 NNBE(T)s occurred at altitudes above 8 km (z ranging from 8.0 to 16.3 km). The plan locations of the 24 NNBE(T)s are shown in Fig. 1a (as orange squares); all were located within 60 km horizontal distance of the EE site.

Fig. 2 shows one example from among the 24 NNBE(T)s. The NNBE (T) shown was isolated in time and space from other lightning events and occurred at an altitude of 15.7 km. It had a range normalized fast antenna amplitude of −17.1 V/m (the largest of the 24 NNBE(T)s) and a VHF power of 5590 W, the third largest VHF power in the group of 24 NNBE(T)s. The NNBE(T) in Fig. 2 had a simple bipolar waveform (Type A in the classification scheme of Karunarathne et al. (2015)); the rise-time of the coincident Log-RF pulse was approximately 1.3 μs.

2.5. Identification of NNBEs preceding -CG flashes

Finding NNBEs associated with the beginning of -CG flashes was more difficult with an automated routine because NNBEs and -CG return strokes both have a large negative-going pulse in the fast antenna data. However, due to the report by Rison et al. (2016) that NNBEs initiate negative -CG flashes, we were motivated to search for such events in our 2016 dataset. In brief, the multistep procedure used to

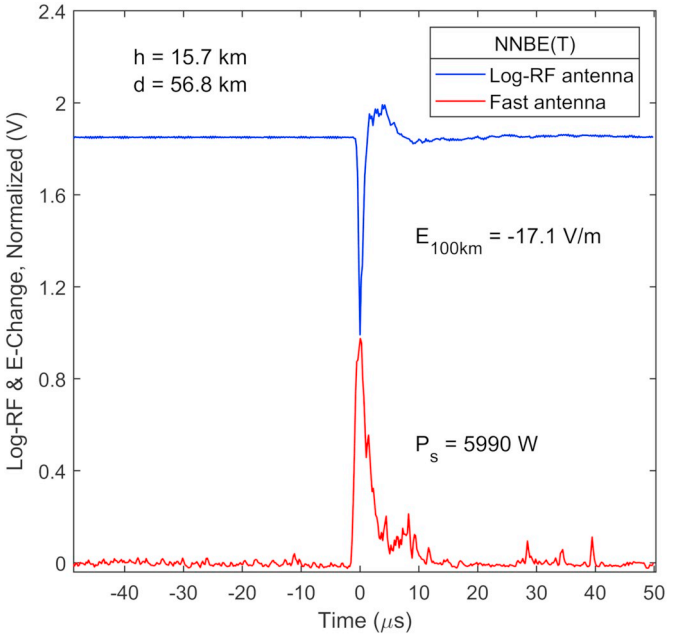

Fig. 2. E-change (FA) and Log-RF waveforms of a typical negative narrow bipolar pulse, NNBE(T), that occurred at an altitude h = 15.7 km and a horizontal range d = 56.8 km from the sensor site. FA data (blue, uncalibrated linear scale) and Log-RF data (red, uncalibrated logarithmic scale) plotted as normalized voltage versus time (i.e., for each curve the largest peak-to-peak pulse amplitude is scaled to 1.0 V). E_{100km} is the FA zero-to-peak amplitude (in V/m) of the NNBE(T) range-normalized to 100 km, while P_S is the VHF power (in watts) of the NNBE(T). (For interpretation of the references to color in this figure legend, the reader is referred to the web version of this article.)

find NNBEs initiating -CG flashes was as follows. Using all triggered fast antenna events from the EE station, the procedure first found triggers that included -CG return strokes, then found the first return stroke of each flash, and then looked for IB pulses before the first return stroke of each flash. At this stage, the procedure yielded a group of -CG flashes with detectable IB pulses. Next, we reduced this group of -CG flashes to those that also had triggered data at five or more sensor sites, so that we could use either PBFA or $\int dE/dt$ to locate NNBEs and IB pulses. Applying this procedure for all the data collected from July and August 2016, gave a total of 1279 -CG flashes with detectable IB pulses and with triggered data from at least five sensor sites.

As in the case for the NNBE(T)s, for further analysis we again focused in on only the NNBEs with horizontal location errors Δx and Δy < 2 km and chi squared goodness-of-fit values < 5. These criteria reduced the sample to a set of 868 -CG flashes. Visual inspection of the 868 -CG flashes yielded 18 cases in which the first IB pulse was preceded by an initiation event in the fast antenna data that was easily identified as an NNBE(L). The NNBE(L)s were defined as follows: each was the initial event in the fast antenna data, each had the characteristic fast antenna bipolar waveform of an NBE, each had a duration in the range of 12–38 μs, and each had a coincident peak in the Log-RF data that was the strongest peak or one of the strongest peaks in the Log-RF data. Example NNBE(L)s are presented in Figs. 3 and 4 and are discussed below. Visual inspection of the 868 -CG flashes also yielded another 15 -CG flashes whose IB pulses were preceded by hump-like NNBE(H)s in the fast antenna data. The NNBE(H)s were defined as follows: each was the initial event in the fast antenna data, each had the "more monopolar" waveform described by Rison et al. (2016) rather than the typical bipolar NBE waveform, each had a duration in the range of 8–21 μs, and each had a coincident with Log-RF peak that was relatively large, though generally weaker in power than the NNBE(L)s. Two NNBE(H) examples are presented in Figs. 5 and 6 and discussed below.

Thus, we found 18 NNBE(L)s and 15 NNBE(H)s in the group of 868 -CG flashes, so only about 4% of the -CG flashes were preceded by a NNBE. Below we show that these 33 flashes were apparently initiated by the NNBEs.

Unlike the NNBE(T)s, the 15 NNBE(H)s and 18 NNBE(L)s all occurred at altitudes below 8.0 km (4.5–7.8 km). Fig. 1b shows the plan position of the first return stroke of the 868 -CG flashes (mostly marked in gray); the 33 -CG flashes preceded by NNBE(H)s or NNBE(L)s are marked in green and purple, respectively. If D is the horizontal distance of a flash location from the EE site, then the 868 -CG flash locations were bounded by 12 km < D < 125 km. The effective upper limit of flash distances in this set is due to the requirement that the IB pulses were detected at 5 or more sites, while the effective lower limit is due to the fact that our identification procedure did not work if the first return stroke saturated the EE fast antenna, as happened at shorter ranges.

Fig. 3 shows one of the 18 NNBE(L)s; this NNBE(L) had the largest VHF power in the group of 18. Fig. 3a shows 10 ms of data, including 5 ms before the initial event of the flash. Based on the $\int dE/dt$ locations (blue dots) of the IB pulses and the NNBE(L), the flash initiated at 6.3 km altitude and developed downward. The identification of the initial event as an NNBE(L) is based in part on its clear bipolar fast antenna pulse and the coincident Log-RF pulse that was larger than any of the Log-RF pulses associated with the IB pulses. Despite having the largest Log-RF pulse, the NNBE(L) did not have the largest magnitude FA pulse since Fig. 3a shows that there were many classic IB pulses with larger magnitudes; the largest IB pulse magnitudes were about a factor of 5 larger than the NNBE(L). The NNBE(L) altitude of 6.3 km is typical for -CG flash initiation.

Fig. 3b is an expanded view of the first 1 ms of electrical activity, including the NNBE(L) and first three classic IB pulses. It is easy to see that each classic IB pulse had a coincident, substantial Log-RF pulse and that before the first classic IB pulse there were several narrow IB pulses, including some with substantial Log-RF pulses, as found by Marshall et al. (2019). Note that the first two narrow IB pulses located after the NNBE(L) are not easily visible in the FA data shown in Fig. 3b, but they were observed and located using $\int dE/dt$. Fig. 3b also indicates that the NNBE(L) and the first classic IB pulse were close to each other in time (~390 μs) and space (~80 m); we take these facts as additional indications that the NNBE(L) likely initiated this -CG flash.

In Fig. 3c the NNBE(L) data are plotted on a 100 μs scale. The NNBE (L) had a range-normalized FA amplitude E_{100km} of 1.16 V/m and a VHF power of 1290 W. (These values are a factor of ~15 and ~5 smaller, respectively, than found for the NNBE(T) in Fig. 2). Note in Fig. 3c that the NNBE(L) had a simple bipolar waveform (similar to the NNBE(T) in Fig. 2), and that the risetime of the coincident Log-RF pulse was about 5 μs (slower than for the NNBE(T) in Fig. 2).

Fig. 3d shows the altitudes with error bars of the NNBE(L), of the classic IB pulses (including sub-pulses), and of many narrow IB pulses shown above in Fig. 3b. Overall, Fig. 3d shows that the trend of the IB pulses was to descend in altitude. However, in the first 500 μs after the NNBE(L), most of the IB pulses had altitudes between 6.2 and 6.4 km with overlapping error bars (Δz ≈ ± 200 m). On the other hand, the Δz error bars did not overlap for the 5.7 km altitude of the second classic IB pulse peak at 520 μs and the altitudes of the two small events at 6.3 km that occurred only 20 μs later (at 590 μs). Recall that 6.3 km was the approximate altitude of the NNBE(L).

The histogram in Fig. 3e is for the distribution of times between each pair of successive (located) pulses in Fig. 3d. The first pair is NNBE (L)-IBP1 and the successive IBP-IBP pairs are IBP1-IBP2, IBP2-IBP3, IBP3-IBP4, etc. It is important to note that the 140 μs between the NNBE (L) and the next pulse (black marker in Fig. 3e) was substantially longer than all of the other interpulse intervals. As discussed later, we find that this first pulse pair, i.e., the interval from the NNBE to the next pulse, typically has one of the longest time intervals in all the NNBE(L)s and NNBE(H)s cases.

To summarize, the NNBE(L) in Fig. 3 apparently initiated the

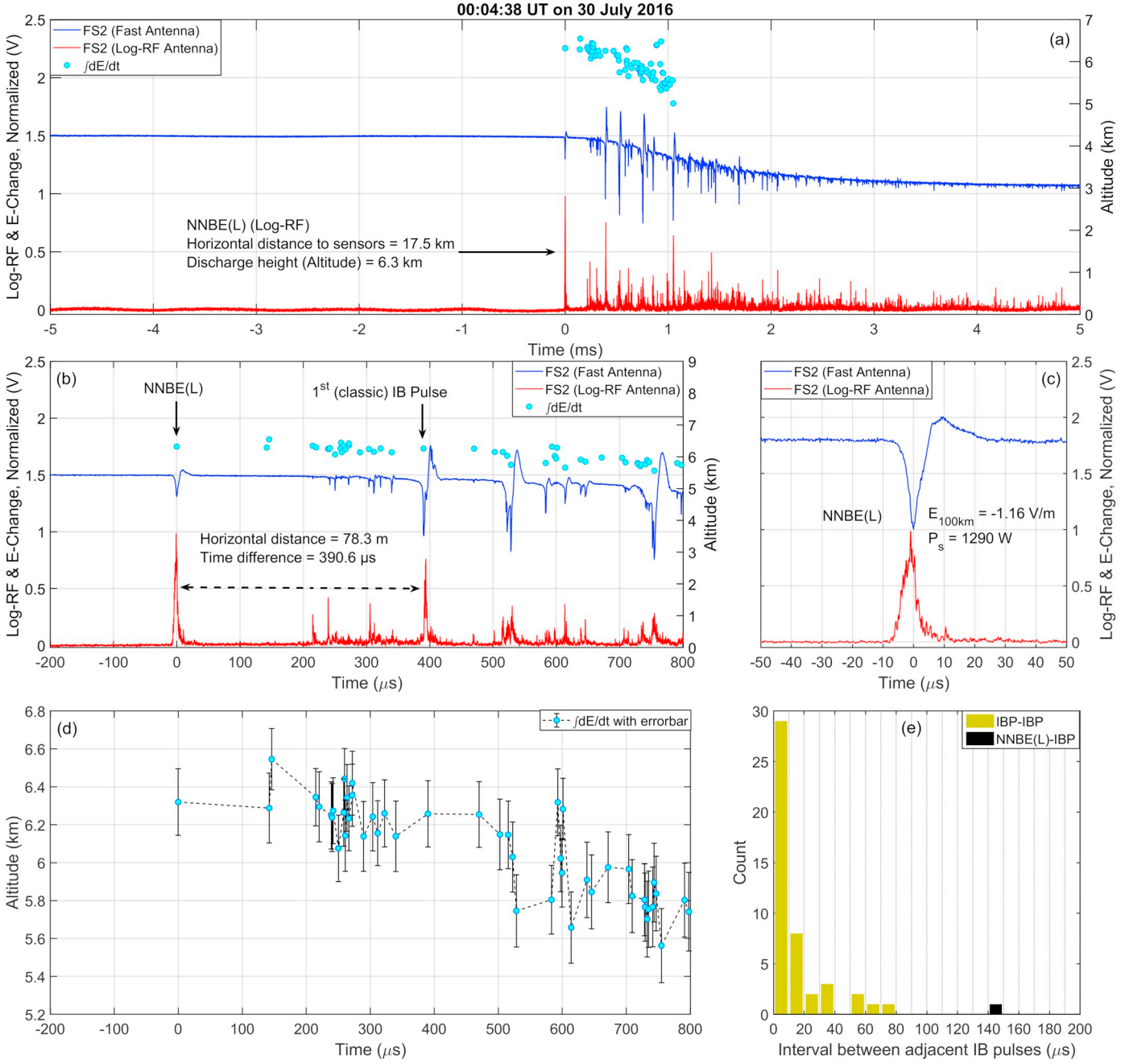

Fig. 3. Example of an NNBE(L) that apparently initiated a -CG flash. The FA data and Log-RF data are both shown as normalized voltages (as in Fig. 2). (a) Overview showing 10 ms of FA data (blue) and Log-RF data (red). Light blue dots represent altitudes (right-hand vertical scale) of FA pulses determined using $\int dE/dt$. Altitude of the NNBE(L) was 6.3 km. (b) Expanded view (1 ms) of first events in (a). (c) Expanded view (100 μs) of the NNBE(L). (d) FA pulse altitudes with error bars for the same 1 ms shown in (b). (e) Histogram of time intervals between successive FA pulses for the same 1 ms shown in (b) and (d). The time interval between the NNBE(L) and the next pulse location is shown in black in the histogram. (For interpretation of the references to color in this figure legend, the reader is referred to the web version of this article.)

following -CG flash, since Fig. 3a shows that there was no electrical activity for at least 5 ms before the NNBE(L), and Fig. 3b shows that the first classic IB pulse occurred only 390 μs after the NNBE(L) and only 80 m horizontally from the NNBE(L). Furthermore, the Log-RF duration of this NNBE(L) was about 12 μs (Fig. 3c), which was typical of the NBEs initiating flashes in Rison et al. (2016). We note that the separation distance of 80 m between NNBE(L) and the first classic IB pulse has an uncertainty of 170 m while their separation in time of 390 μs has an uncertainty < 1 μs.

Fig. 4 is similar to Fig. 3 for another example of an NNBE(L) that apparently initiated a -CG flash. This NNBE(L) had $E_{100km} = -0.23$ V/m and a VHF power of 55 W. Note that the altitude of this NNBE(L) was lower than the following IB pulses with no overlap of altitude error bars (Fig. 4d); this finding and others like it are discussed in Section 3.8.

Fig. 5 shows characteristics for one of the largest of the 15 NNBE(H)s. This event had a hump-like fast antenna pulse (no clear overshoot) with E_{100km} of only −0.17 V/m and a relatively weak, coincident Log-RF pulse with a VHF power of only 12.9 W. Despite this low power, only a few of the IB pulses had larger Log-RF pulses than the NNBE(H) (Fig. 5a and b) even though many of them had substantially larger E_{100km} amplitudes. This NNBE(H) apparently initiated the following -CG flash, since (1) there was no electrical activity before the NNBE(H)

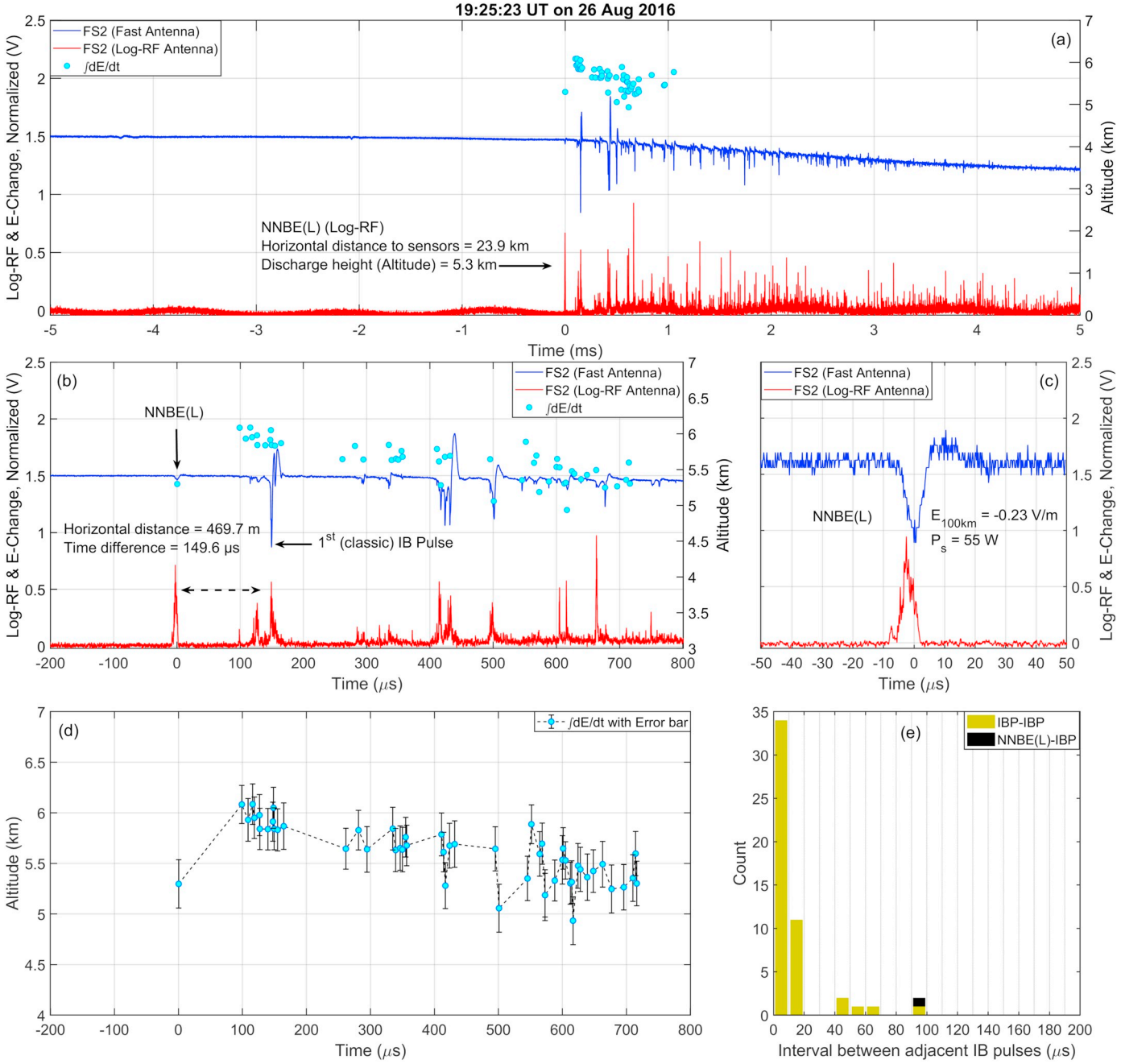

Fig. 4. Similar to Fig. 3, showing another example of an NNBE(L) that apparently initiated a -CG flash.

(Fig. 5a) and (2) the first classic IB pulse occurred about 90 μs after the NNBE(H) and only about 136 m horizontally from the NNBE(H) (Fig. 5b) (with time and distance uncertainties of < 1 μs and 610 m, respectively). Furthermore, the NNBE(H) FA waveform was similar to the two "more monopolar" negative NBEs shown in Rison et al. (2016) that initiated -CG flashes. As in Fig. 3d, Fig. 5d shows that the general trend of the IB pulses was to descend in altitude, that most of the IB pulse altitudes had overlapping error bars ($\Delta z \approx \pm 250$ m), but that some of the higher and lower IB pulse altitudes were separated by > 500 m. Fig. 5e shows that the ~50 μs between the NNBE(H) and the next pulse was longer than all but one of the other interpulse intervals.

Fig. 6 is similar to Fig. 5 and shows another example of an NNBE(H) that apparently initiated a -CG flash; this NNBE(H) had E_{100km} of only −0.10 V/m and a VHF power of 4.0 W. Note that the altitude of this NNBE(H) was higher than the first IB pulse with no overlap of altitude error bars. Despite the NNBE(H)'s small amplitude, it was easily detected by five FA sensors, as shown by Fig. A1 in Appendix A.

In summary, among the set of 868 -CG flashes, each of the 18 NNBE (L)s and 15 NNBE(H)s were identified as initiating –CG flashes because they satisfied the following criteria, as seen in the examples in Figs. 3, 4, 5, and 6:

(a) The NNBE was the first event of a -CG flash. In other words, the change from no electrical activity to electromagnetic pulses of the -CG flash began with the NNBE.
(b) The NNBE was close in time (average 220 μs) and close in space (average 300 m) to the first classic IB pulse of the -CG flash; details of these values are given later (Section 3.6). Although the flashes studied herein were too far from the FA sensors to detect an IEC, the NNBE probably started an IEC that led to the first classic IB pulse (e.g., Marshall et al., 2014; Chapman et al., 2017).
(c) The NNBE(L)s had a simple bipolar FA waveform and a Log-RF

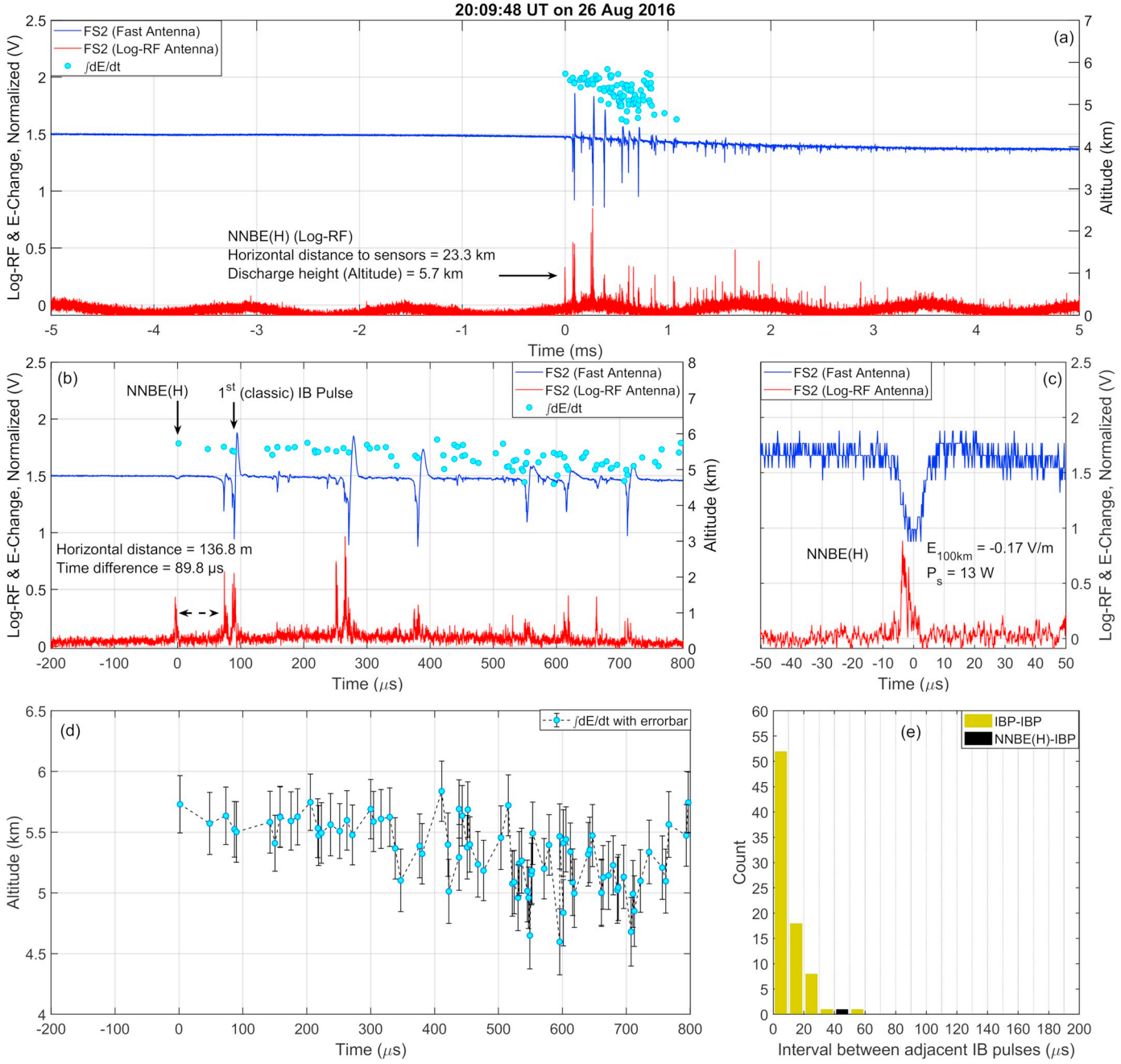

Fig. 5. Similar to Fig. 3, showing an example of an NNBE(H) that apparently initiated a -CG flash.

power that was larger than the power of all or almost all of the IB pulses.

(d) The NNBE(H)s had a small amplitude hump-like FA waveform and a Log-RF power that was quite large relative to the E_{100km} amplitude of the FA hump.

Obviously, finding only 33 –CG flashes were initiated by NNBEs leaves 835 -CG flashes that must have initiated without an NNBE, similar to the two -CG flashes investigated in Marshall et al. (2019).

3. Statistical results

In this section we report findings based on the dataset of 868 -CG flashes and on statistical analyses of the 24 NNBE(T)s, 18 NNBE(L)s, and 15 NNBE(H)s, described above, with Δx and $\Delta y < 2$ km and chi squared goodness-of-fit values < 5.

3.1. Low percentage of -CG flashes preceded by an NNBE

As discussed in Section 2.5, visual inspection of the beginning of each flash in the group of 868 -CG flashes with detectable and locatable IB pulses determined that there were 33 NNBE(L)s and NNBE(H)s. Thus, we found that only 4% of the 868 -CG flashes were preceded by and probably were initiated by an NNBE. Based on this finding, it seems likely that most (i.e., about 96%) of the -CG flashes that occurred during our data collection were not initiated by an NNBE. This finding is similar to the finding of Lyu et al. (2019) that only about 10% on IC flashes were initiated by a positive NBE. It is important to note that the Lyu et al. (2019) data were collected on flashes within 10 km of their interferometer, so there was no chance of missing the NBE signature. If the percentage of -CG flashes initiated by NNBEs is similar to the percentage of IC flashes initiated by positive NBEs found by Lyu et al. (2019), then it is likely that we detected a significant fraction of the

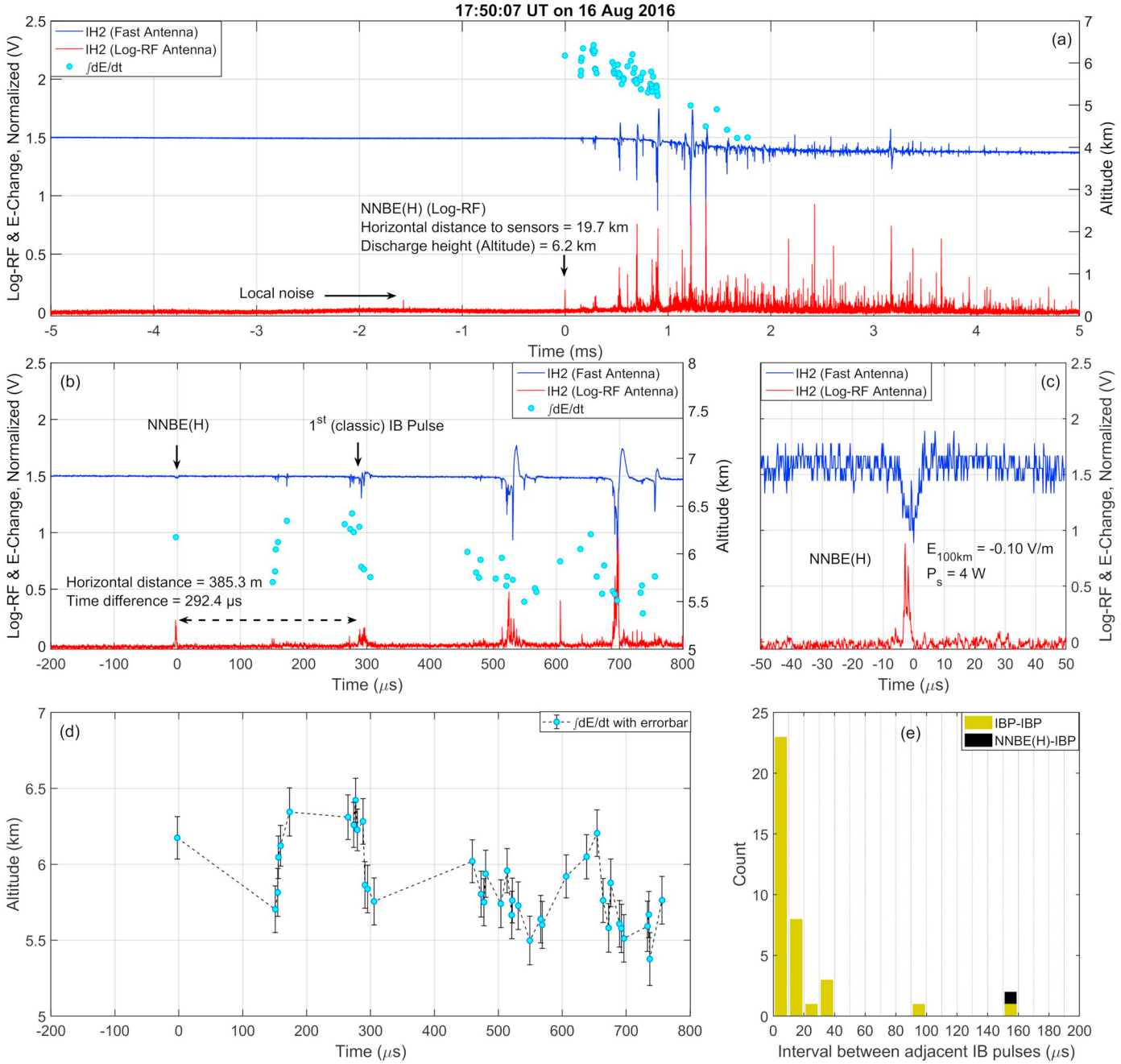

Fig. 6. Similar to Fig. 5, showing another example of an NNBE(H) that apparently initiated a -CG flash.

NNBEs initiating -CG flashes in our group of 868 -CG flashes.

3.2. Altitudes of NNBEs

Fig. 7a shows the altitude distribution of 24 NNBEs(T), 18 NNBEs (L), and 15 NNBE(H)s. The altitudes of the 24 NNBE(T)s ranged from 8.0 to 16.3 km with average of 12.2 km, while the 18 NNBE(L)s ranged from 5.0 to 7.5 km with average of 6.27 km, and 15 NNBE(H)s ranged from 4.6 to 7.8 km an average of 6.18 km.

In Fig. 7a we also see that the NNBE(L)s and NNBE(H)s occurred in the same altitude range despite their different fast antenna waveforms. Rison et al. (2016) showed two events like our NNBE(H)s (their Fig. 4c and d) that occurred at 6.0 km altitude and initiated -CG flashes. Rison et al. (2016) seemed to suggest that despite their "more monopolar" waveforms, these events were true negative NBEs, since they were caused by fast positive breakdown, just like the more powerful positive NBEs (with bipolar waveforms) that initiated the IC flashes in that study. Therefore, the fact that the NNBE(L)s and NNBE(H)s spanned similar altitudes in Fig. 7a is consistent with the possibility that NNBE (H)s are merely low power variants of NNBE(L)s.

The altitudes of 21 of the 24 NNBE(T)s in this study were below 15 km and thus lower than the majority of those found by Smith et al. (2004) and Wu et al. (2012). The average altitude of our 24 NNBE(T)s is 5–6 km lower than averages reported in those two earlier studies. The NNBE(L)s and NNBE(H)s occurred at even lower altitudes than the NNBE(T)s in this study, which is not surprising since each of these NNBEs was the initial event of a -CG flash. Overall, Fig. 7a shows that the NNBE(L)s and NNBE(H)s in this study had no altitude overlap with the vast majority of typical, high altitude NNBE(T)s found in this and in earlier studies.

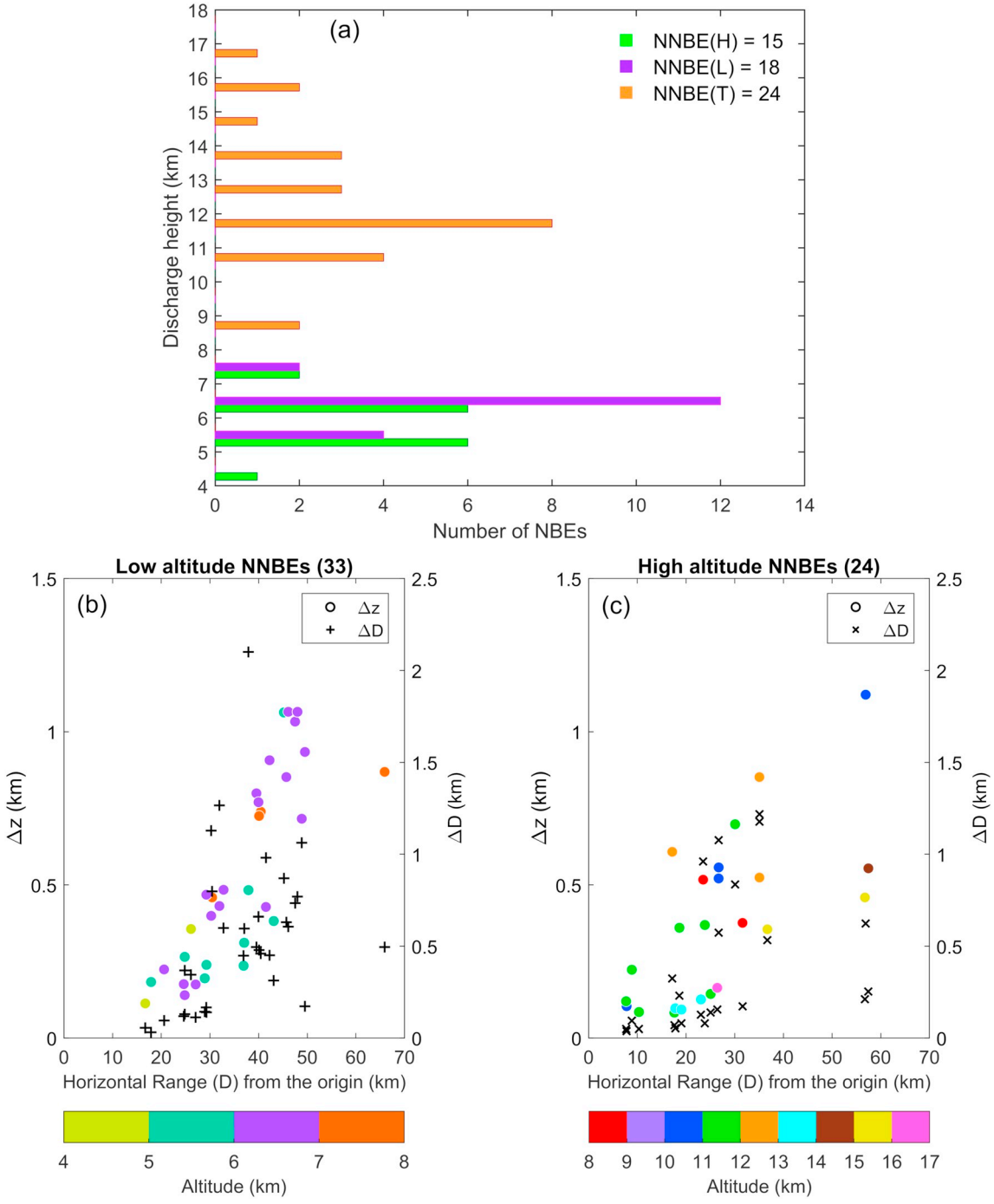

Fig. 7. (a) Altitude histogram of the three types of NNBEs. (b) Horizontal distance error (Δ*D*) and altitude error (Δz) for NNBEs initiating CG flashes, namely NNBE(L)s and NNBE(H)s, versus NNBE horizontal range, D. Each NNBE has a colored circle for Δz and a "+" for ΔD. These NNBEs occur at altitudes below 8 km with altitudes indicated by the color bar. (c) Similar to (b), but for NNBE(T)s versus NNBE horizontal range. These NNBEs occur at altitudes above 8 km with altitudes indicated by the color bar. (For interpretation of the references to color in this figure legend, the reader is referred to the web version of this article.)

Fig. 7b shows the horizontal location errors, ΔD, and the altitude location errors, Δz, for the low altitude NNBEs (i.e., NNBE(L)s and NNBE(H)s); Fig. 7c shows ΔD and Δz for the high altitude NNBE(T)s. All 57 of the selected NNBEs had $\Delta z < 1.2$ km and (with one exception) had $\Delta D < 1.4$ km. As expected for time-of-arrival locating techniques (e.g., the PBFA algorithm used herein), Fig. 7b and c show that altitude errors increase with horizontal range to the flash but are generally smaller for higher altitude events (e.g., Karunarathne et al., 2013).

3.3. Durations of NNBEs

Fig. 8a shows a histogram of the total pulse durations for the three types of NNBEs based on fast antenna data collected at distances > 20 km with durations determined using the method of Nag et al. (2009). For each NNBE type, the arithmetic mean with its standard deviation and geometric mean with its standard deviation are given. The arithmetic mean durations for NNBE(H), NNBE(L), and NNBE(T) were 13, 25, and 20 μs, respectively. The NNBE(L) and NNBE(T) durations are in reasonable agreement with an arithmetic mean of 25 μs

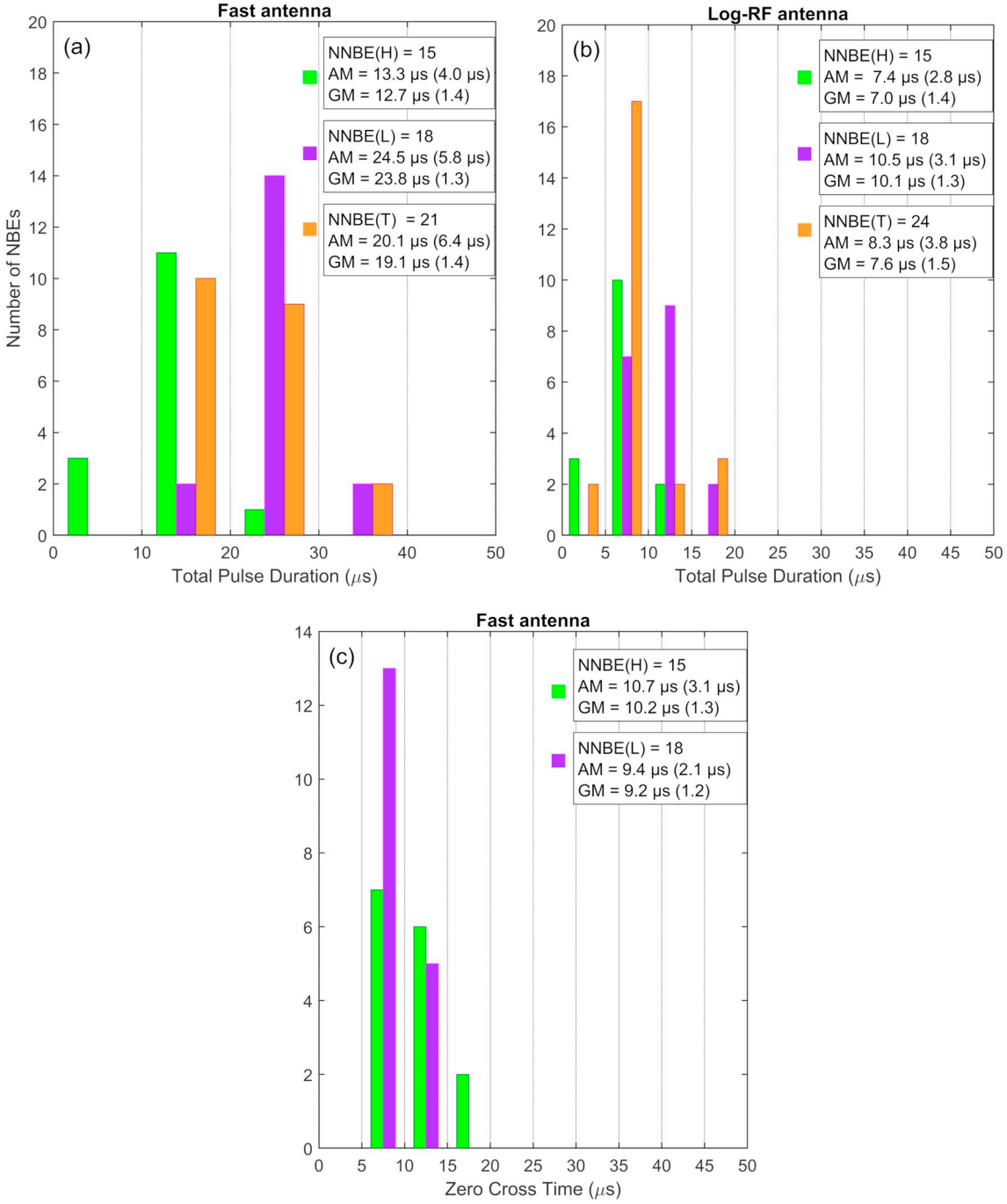

Fig. 8. (a) Durations for the three NNBE types, based on FA data at distances > 20 km. (b) Durations for the three NNBE types, based on Log-RF data. (c) Zero cross time based on FA data for NNBE(L)s and NNBE(H)s; equivalent to the durations of the leading pulse of the NNBE(L) bipolar pulses and the durations of the hump in NNBE(H) pulses. The legend of each plot includes the arithmetic mean (AM) with the standard deviation in parentheses plus the geometric mean (GM) with its standard deviation in parentheses. The grid lines in each figure show the bin edges.

reported by Azlinda Ahmad et al. (2010) for 75 negative narrow bipolar pulses. The approximately 50% shorter pulse durations for NNBE(H) may be due to their lack of an overshoot pulse. Thus, these duration data are consistent with the notion that NNBE(H)s are weak variants of NNBE(L)s in which the overshoot pulse is so weak it is lost in the noise. An alternate explanation is that NNBE(H)s develop via a different mechanism from NNBE(L)s that does not produce any overshoot pulse.

Fig. 8b is a histogram of the duration of the main peak of the Log-RF waveform associated with NNBEs. Relevant Log-RF data were obtained by averaging measurements from at least 4 sensor sites. The arithmetic mean durations for NNBE(H), NNBE(L), and NNBE(T) were 7, 11, and 8 μs, respectively. The NNBE(H) average duration of 7 μs was shorter than the durations of 10 and 14 μs for two NNBE(H)s reported by Rison et al. (2016). Overall, the durations of the Log-RF pulses were about half the durations of the coincident fast antenna NNBE pulses (Fig. 8a). For most NNBEs, the main Log-RF pulse occurred during the initial half cycle of the bipolar fast antenna pulse or during the fast antenna hump in the NNBE(H)s, which fits with the Log-RF pulse durations being about half of the fast antenna pulse durations.

Fig. 8c is a histogram for the “zero cross time” of NNBE(L)s and NNBE(H)s, by which we mean the durations of the initial half cycle of the FA bipolar waveform for NNBE(L)s (e.g., Willett et al., 1989) and

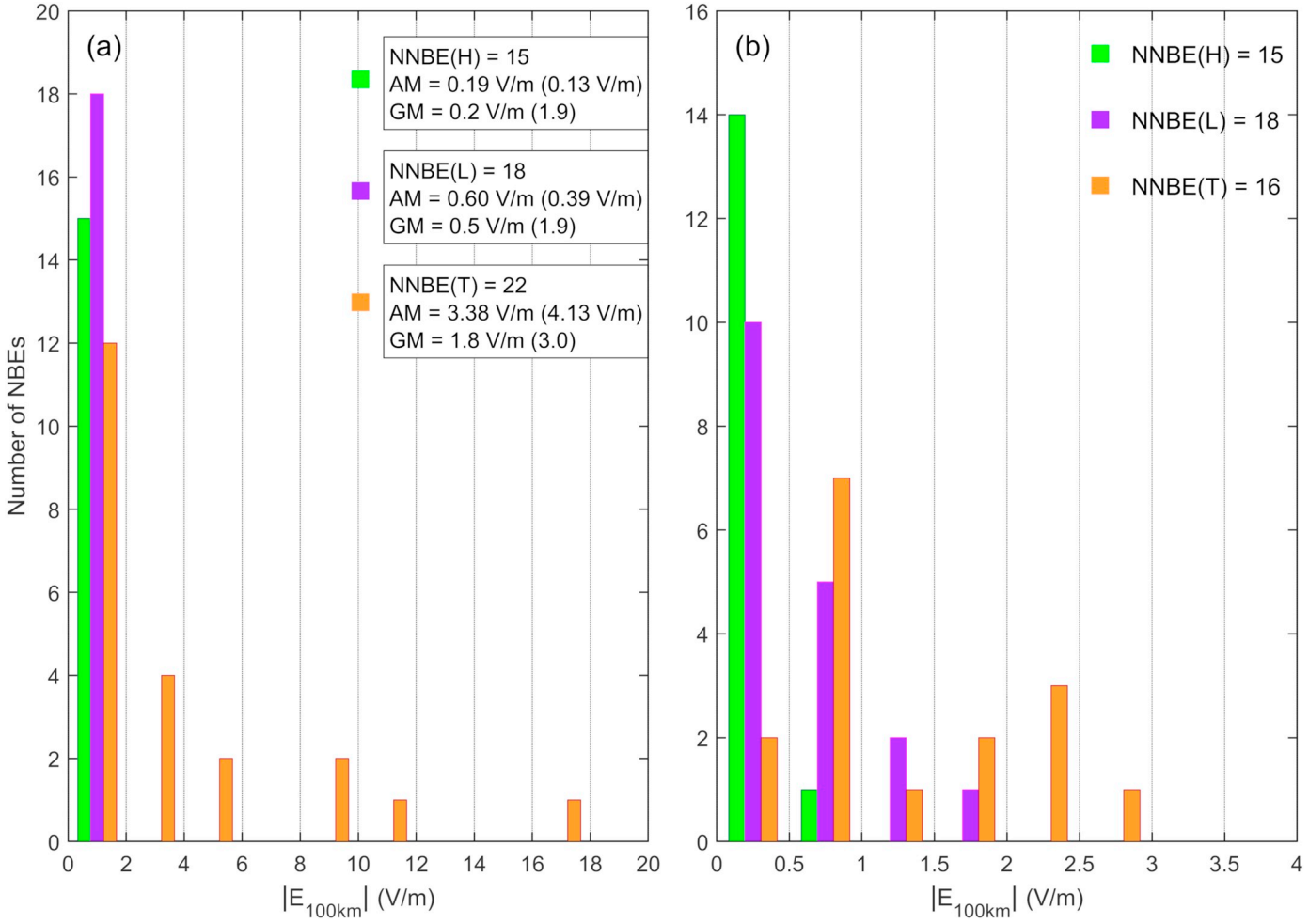

Fig. 9. (a) Histogram of NNBE zero-to-peak FA magnitudes range-normalized to 100 km (E_{100km}) for the three NNBE groups. The legend includes the arithmetic mean (AM) with the standard deviation in parentheses plus the geometric mean (GM) with its standard deviation in parentheses. The vertical grid lines show the bin edges. (b) Expanded view of data from 0 to 4 V/m.

the durations of the hump for NNBE(H)s. The similar zero cross times for NNBE(L)s and NNBE(H)s seen in Fig. 8c are consistent with the idea that NNBE(H)s may be weak variants of NNBE(L)s. However, if the NNBE(H)s are produced by a different mechanism from the NNBE(L)s that does not produce an overshoot peak, then the "zero cross times" defined for NNBE(H)s would be meaningless in comparison to a bipolar waveform.

3.4. Range-normalized amplitudes of NNBEs

Fig. 9a presents a histogram of range-normalized electric field changes, E_{100km}, of 15 NNBE(H)s, 18 NNBE(L)s, and 22 NNBE(T)s; the histogram spans E_{100km} values from 0 to 20 V/m. Fig. 9b is an expanded histogram showing only those E_{100km} values that are < 4 V/m, which includes all of the NNBE(H)s and NNBE(L)s and 16 NNBE(T)s. In order to avoid electrostatic effects, only NNBEs that occurred at horizontal ranges > 20 km from the EE sensor were included in this analysis. E_{100km} for 15 NNBE(H)s ranged from 0.06 to 0.54 Vm^{-1} with an arithmetic mean of (0.19 ± 0.13) Vm^{-1}. E_{100km} for 18 NNBE(L)s varied from 0.15 to 1.53 Vm^{-1} with an arithmetic mean of (0.60 ± 0.39) Vm^{-1}. E_{100km} for 22 NNBE(T)s varied from 0.41 to 16.21 Vm^{-1} with an arithmetic mean (3.38 ± 4.13) Vm^{-1}. The arithmetic mean of E_{100km} values of NNBE(T)s in this study were much smaller than the corresponding NNBE arithmetic mean of (17.6 ± 7.1) Vm^{-1} reported by Azlinda Ahmad et al. (2010) for thunderstorms in Malaysia. Overall, the E_{100km} values of NNBEs found herein indicate that the NNBE(L)s were significantly larger than the NNBE(H)s, but both of these low-altitude NNBE types had substantially smaller E_{100km} values than most NNBE(T)s.

The data in Fig. 9 also are consistent with the idea that NNBE(H)s are weaker, lower power variants of NNBE(L)s despite their different fast antenna waveforms. Since Fig. 9 shows that NNBE(H) fast antenna waveforms have smaller E_{100km} values than NNBE(L)s, the NNBE(H)s may "lack" the overshoot because it is lost in the fast antenna noise. One fact supporting this explanation is that the ratio of the NBE bipolar initial half cycle to its overshoot is generally relatively large, varying from about 3 to 9 (e.g., Willett et al., 1989; Azlinda Ahmad et al., 2010). The combination of this typical ratio with a weak initial half cycle of an NNBE(H) could make any NNBE(H) overshoot difficult to detect, even if the physical mechanism that produces the NNBE(H)s and NNBE(L)s is the same.

3.5. VHF power of NNBEs

Fig. 10 shows distributions of radiated peak source power for NNBE (H)s, NNBE(L)s, and NNBE(T)s, estimated according to Eq. (1) using Log-RF data collected in the 186–192 MHz band. The Log-RF powers of the 15 NNBE(H)s ranged from 1 to 23 W with an arithmetic mean of 7.6 W (or 8.8 dBW). The Log-RF powers of the 18 NNBE(L)s ranged from 9 to 1290 W with an arithmetic mean of 232 W (or 23.7 dBW). The Log-RF powers of the 24 NNBE(T)s ranged from 260 to 7420 W with an arithmetic mean of 1770 W (or 32.5 dBW). Thus, the NNBE(H)s had the weakest VHF powers, the NNBE(L)s were more powerful, and the NNBE

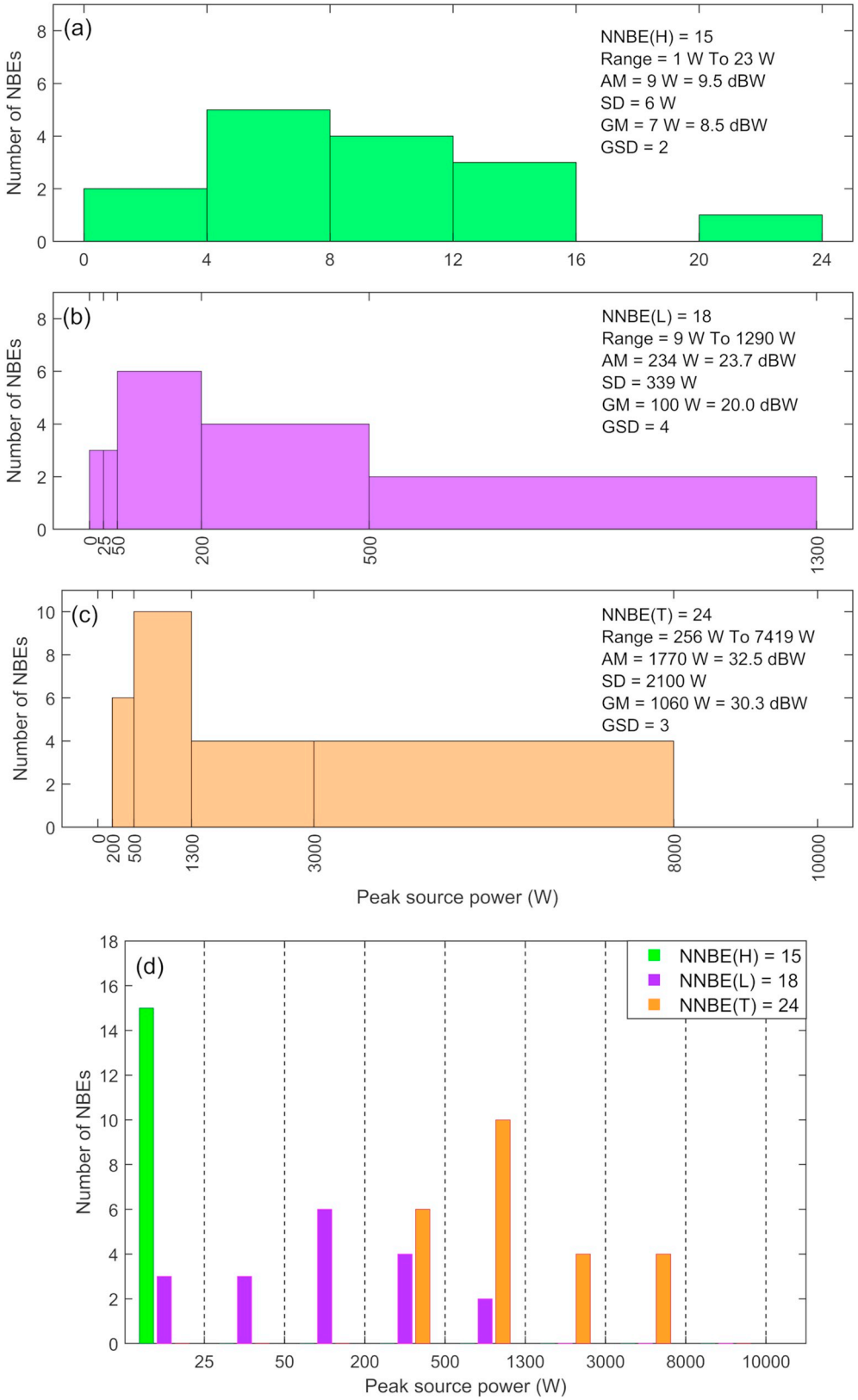

Fig. 10. Histograms of VHF powers of the three NNBE types. Note the different bin sizes in each histogram. (a) NNBE(H)s. (b) NNBE(L)s. (c) NNBE(T)s. (d) Comparison histogram showing all three types of NNBEs; bin edges are shown by the vertical dashed lines. AM = arithmetic mean, SD = standard deviation of AM, GM = geometric mean, GSD = standard deviation of GM.

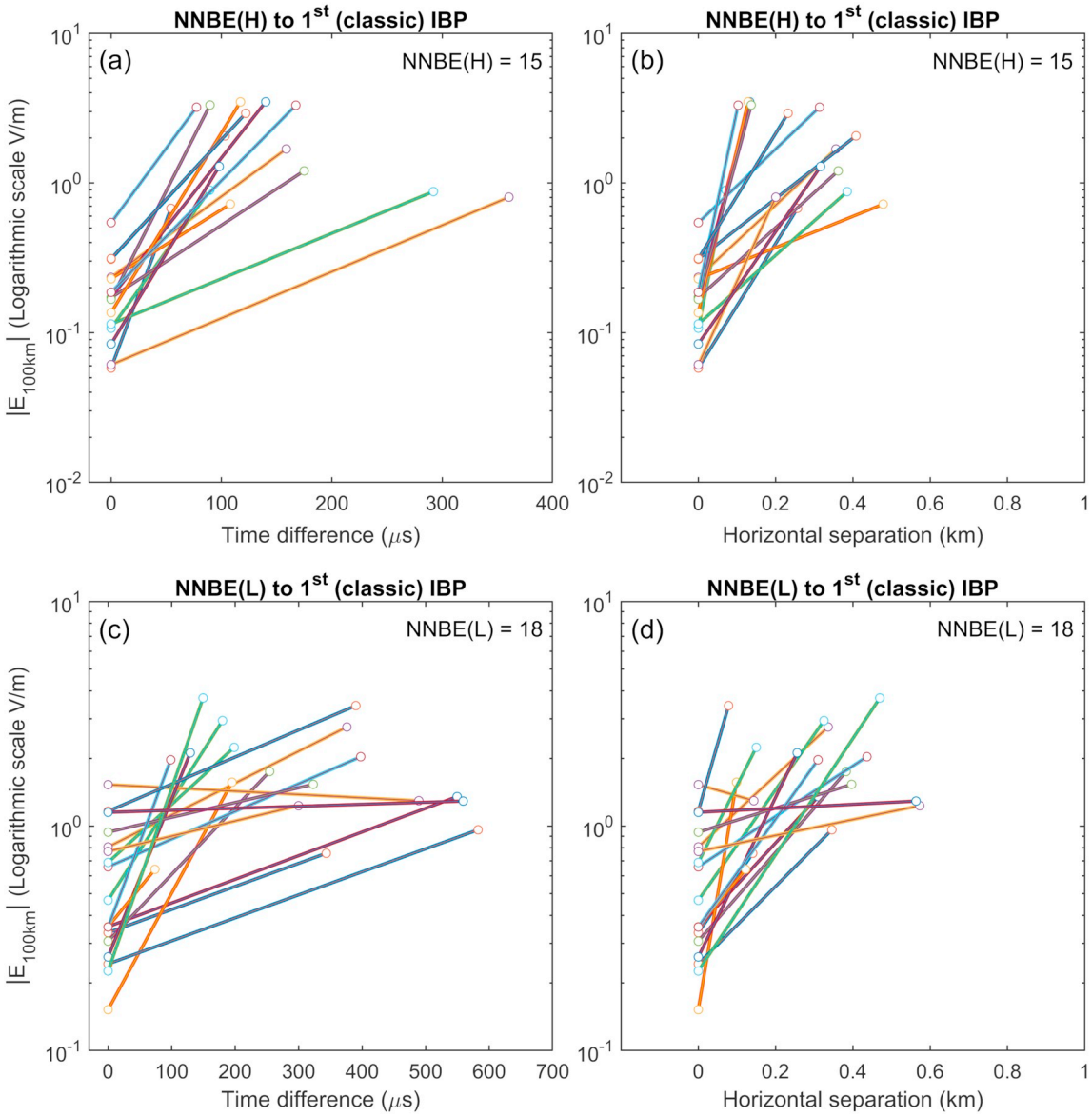

Fig. 11. Distance and time separations between NNBEs and the first classic IB pulse with (a) and (b) showing values for 15 NNBE(H)s and with (c) and (d showing values for 18 NNBE(L)s. In each frame the NNBE is plotted at zero on the horizontal axis (time difference or horizontal distance difference) and plotted on the vertical axis with the NNBE's range-normalized peak amplitude (E_{100km}). In each frame the 1st IBP of the CG flash initiated by the NNBE is plotted in the horizontal with the time of occurrence after the NNBE or horizontal distance from the NNBE and plotted on the vertical axis with the 1st IBP's E_{100km} amplitude.

(T)s were substantially more powerful. For comparison Rison et al. (2016) showed two NNBEs that initiated -CG flashes; their VHF powers were 9.0 and 25.8 dBW and were detected in the 60–66 MHz band.

3.6. Distance and time separations between NNBEs and the first classic IB pulse

We analyzed the 15 NNBE(H)s and 18 NNBE(L)s that initiated -CG flashes to find the time separation and the horizontal distance separation between each of the NNBEs and the first classic IB pulse (or 1stCIBP) of the -CG flash. Note that this time separation is, by definition, the duration of the IEC that occurs at the beginning of most or all flashes (Marshall et al., 2014; Chapman et al., 2017). For 15 NNBE(H)s Fig. 11a shows the time separation in μs (horizontal axis) for each NNBE(H)/1stCIBP pair plotted as a line connecting the NBBE(H) at 0 μs and the 1st CIBP at the time it occurred after the NNBE(H). The vertical axis in Fig. 11a shows the range-normalized E_{100km} amplitudes of the NNBE(H) and the 1stCIBP, so each NNBE(H) or 1stCIBP is plotted as a (time, E_{100km}) point. The time separations of NNBE(H)/1stCIBP pairs varied from 27 to 368 *μs*, with an average value of 136 *μs* and an uncertainty < 1 μs. It can be seen from the Fig. 11a that most of the 1stCIBPs occurred < 200 μs after their corresponding NNBE(H)s. These time separations are in good agreement with the durations of IECs at the beginning of -CG flashes in Florida thunderstorms, which had average durations of 180 μs and 230 μs (Marshall et al., 2014; Chapman et al., 2017, respectively). Fig. 11b is similar to Fig. 11a, but shows that the horizontal distance separation of NNBE(H)/1stCIBP pairs varied from 70 to 500 m with an average of 300 m. Note however, that the separation uncertainty was usually 100–300 m with a maximum of ~600 m. The short time separations and close distance separations support the hypothesis that the NNBE(H)s initiated these 15 -CG flashes. Note also in Fig. 11a and b that the E_{100km} amplitudes of all NNBE(H)s are smaller than the E_{100km} amplitudes of the 1stCIBPs, which emphasizes how small the NNBE(H) E_{100km} amplitudes are in these data.

Fig. 11c and d are similar in layout to Fig. 11a and b, but are instead

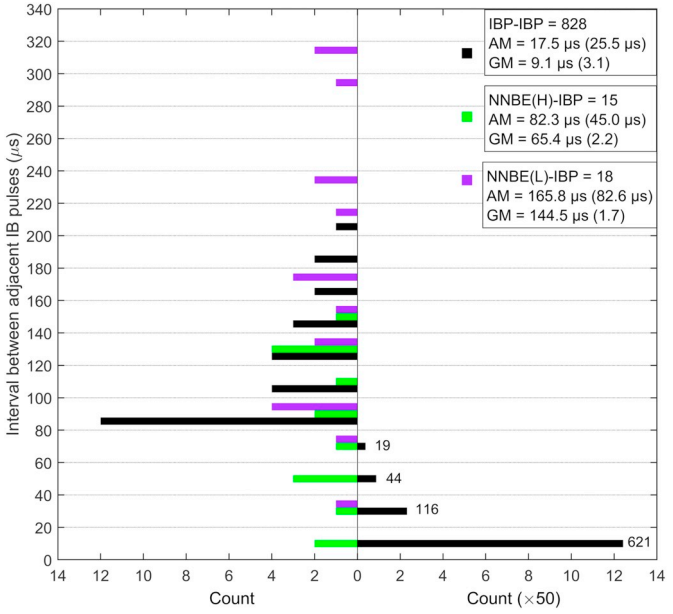

Fig. 12. Histogram of time separations between successive pulses; examples of these separations are shown in Figs. 3d, e and 4d, e. Three groups of time separations are shown: (i) for 15 flashes, the time separation between the initiating NNBE(H) and the following IBP (marked in green), (ii) for 18 flashes, the time separation between the initiating NNBE(L) and the following IBP (marked in purple), and (iii) 828 IBP-IBP time separations that occurred after the NNBE-IBP pair during first millisecond of 10 NNBE(H)s and 10 NNBE(L)s (marked in black). Bin edges are shown by the horizontal lines; the legend for each group includes its arithmetic mean (AM) with the standard deviation in parentheses plus its geometric mean (GM) with standard deviation in parentheses. (For interpretation of the references to color in this figure legend, the reader is referred to the web version of this article.)

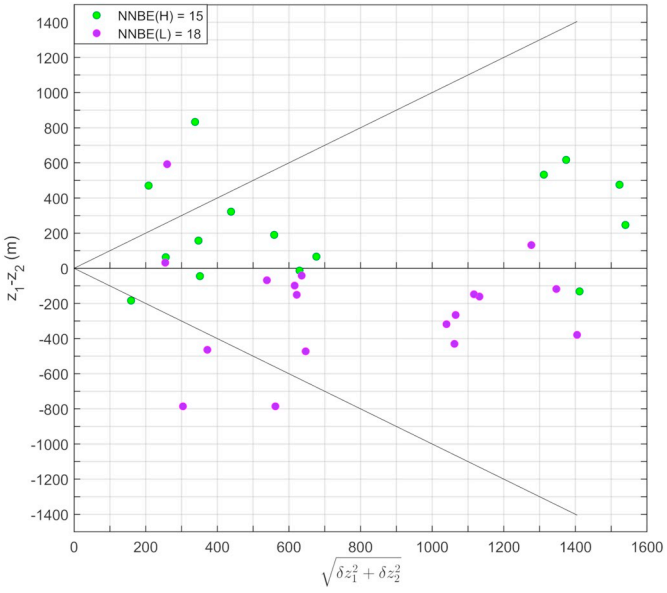

Fig. 13. Altitude difference (z_1–z_2) between the initiating NNBE and the first IB pulse in the flash, plotted as a function of the estimated error in the altitude difference. Solid diagonals are unity ratios. Points above (below) zero are events for which the NNBE is higher (lower) than the first IB pulse. The three NNBE-firstIB pairs above the upper diagonal and the four NNBE-firstIB below the lower diagonal had altitude differences (z_1–z_2) greater in magnitude than the estimated combined altitude error.

for 18 NNBE(L)/1stCIBP pairs. It is immediately obvious (because of the negative slope of some connecting lines) that some NNBE(L)s had larger E_{100km} amplitudes than the corresponding 1stCIBP. In Fig. 11c the separation time of NNBE(L)/1stCIBP pairs was on average longer than for NNBE(H)/1stCIBP pairs with the separation times ranging from 74 to 583 μs with an average of 311 μs, which is somewhat larger than the IEC average duration of 230 μs in Chapman et al. (2017). The time uncertainty is again < 1 μs. Fig. 11d shows horizontal distance separation of NNBE(L)/1stCIBP pairs varied from 60 to 600 m with an average value of 300 m, which was equal to the average separation distance of NNBE(H)/1stCIBP pairs. Overall, the relatively short time separations and relatively close distance separations support the hypothesis that the NNBE(L)s initiated these 18 -CG flashes.

3.7. Successive time separations between FA pulses

In Figs. 3e, 4e, 5e, and 6e we showed that the time separation between the NNBE and the following narrow IBP (the NNBE-IBP pair) was usually longer than the time separations between the following successive IBP-IBP pairs. In Fig. 12 we investigate this tendency. Fig. 12 shows histograms of time separations for three groups: (1) the 15 NNBE (H)-IBP pairs, (2) the 18 NNBE(L)-IBP pairs, and (3) 828 IBP-IBP pairs from 10 of the NNBE(H) flashes and 14 of the NNBE(L) flashes. The third group of pairs is taken from the first 800 μs from each flash, as shown for example in Fig. 3d and e, which has 45 IBP-IBP pairs. On average for 24 -CG flashes, there were 37 IBP-IBP pairs in the first 800 μs.

Fig. 12 shows that 621 of 828 or 75% of the IBP-IBP pairs had time separations < 20 μs. The arithmetic mean (AM) separation of the 828 IBP-IBP pairs was 17.5 μs with the largest separation being < 220 μs. The time separation of the 15 NNBE(H)-IBP pairs averaged 82.3 μs, while the time separation of the 18 NNBE(L)-IBP pairs averaged 165.8 μs. Both NNBE-IBP average times were significantly longer than the IBP-IBP times. Thus the interval after the NNBE is different than the interpulse intervals during the IB stage.

3.8. Altitude separations between NNBE-IBP

In Rison et al. (2016), the positive NBEs that initiated IC flashes had fast positive breakdown moving downward followed by negative discharges moving upward. We examined our dataset for the opposite directional development in the -CG flashes initiated by NNBEs. It was found that after the NNBEs the general trend of the IB pulses was to move negative charge downward (see Figs. 3a, 4a, 5a, and 6a). However, because of the relatively large altitude errors for our NNBEs and IB pulses, what is less certain is the position of the NNBE relative to the following IB pulse. For example Fig. 3d shows that the NNBE(L) altitude, including its uncertainty, was about the same as the altitude of the IB pulse that immediately followed the NNBE(L); however, even considering their altitude error bars, Fig. 4d showed that the NNBE(L) altitude was below the following IB pulse. Similarly, in Fig. 5d the NNBE (H) altitude was about the same as the following IB pulse but the NNBE (H) in Fig. 6d was clearly above than the following IB pulse.

Fig. 13 shows, for the 15 NNBE(H)s and 18 NNBE(L)s, the altitude difference ($z_1 - z_2$), where z_1 is the NNBE altitude and z_2 is the first IB pulse altitude, versus the uncertainty in this difference. Positive values of ($z_1 - z_2$) indicate the NNBE was above the first IB pulse, as expected for –CG flash initiations based on Rison et al. (2016). At first glance, there is an intriguing tendency for the NNBE(L)s to be lower than the first IB pulse and the NNBE(H)s to be higher than the first IB pulse. However, the diagonal lines show where the difference ($z_1 - z_2$) is equal to the uncertainty in the difference. Based on these “unity” lines, 26 of the 33 NNBEs were close enough to the IB pulse altitude such that their relative altitude is uncertain. Of the remaining 7 NNBEs, three were above the first IB pulse and four were below the first IB pulse, with a mixture of NNBE types (L and H) in both groups. In our opinion, no solid conclusion about the relative altitudes of NNBEs and the first IB

pulse can be drawn from these data. We hope to study this question further in the future with -CG flashes that are closer to our sensors for which the uncertainties in altitude are smaller.

We are surprised that in Fig. 13 the NNBE(H)s tend to have higher altitudes than the first IB pulse that follows them, and that the NNBE(L)s have the opposite tendency relative to the first IB pulse that follows them. We have no explanation of this apparent difference in tendency. The planned future work will also provide a test of this preliminary observation.

4. Discussion

NBEs are supposed to be very strong VHF radiators (e.g., Le Vine, 1980); Rison et al. (2016) reported positive NBEs with powers as large as 274,000 W and 5 NNBEs with powers in the range of 8–380 W. NBEs are also supposed to have large E_{100km} values: Willett et al. (1989) reported the arithmetic mean (AM) for 18 positive NBEs was 8.0 V/m; Karunarathne et al. (2015) reported AM = 11.0 V/m for 226 positive NBEs; Azlinda Ahmad et al. (2010) reported AM = 22.7 V/m for 107 positive NBEs and AM = 17.6 V/m for 75 NNBEs. (Note that the altitudes of the NBEs in Willett et al. and in Ahmad et al. were not determined.) It has also been assumed that the charge motion of NBEs is vertically oriented, and in a study of 10 positive NBEs Karunarathne et al. (2016) showed that 7 were essentially vertical and 3 were oriented at 10°–20° from vertical.

In contrast to expectations, Fig. 10 shows that our NNBE(H)s and NNBE(L)s had AM powers of 9 W and 230 W, respectively, and Fig. 9 shows that the E_{100km} values of our NNBE(H)s and NNBE(L)s had AM values of 0.19 V/m and 0.60 V/m, respectively. We have suggested above that the NNBE(H)s might be weak variants of the NNBE(L)s based on their similar characteristics. We further speculate that NNBE(H)s and NNBE(L)s might propagate with a substantial horizontal component in addition to a vertical component. If this speculation is correct, then the weak VHF powers might be primarily due to θ approaching π/2 rad in Eq. (2) (rather than θ = 0 rad, as assumed). A mainly horizontal orientation could also account for the relatively small E_{100km} values of NNBE(H)s and NNBE(L)s. Some support for this hypothesis is found in Figure 4d of Rison et al. (2016), which shows mainly horizontal fast positive breakdown for an NNBE(H) with an estimated source power of only 8 W. Determination of the current propagation angle can best be accomplished with close examples of NNBEs, thus we will explore the possibility of non-vertical orientations in future work.

5. Summary and conclusions

This study examines negative narrow bipolar events, or NNBEs, that occurred in July and August of 2016 in Mississippi thunderstorms. Our main focus has been on NNBEs that initiated some -CG flashes, called NNBE(L)s and NNBE(H)s herein. For comparison we also examine typical, high altitude NNBEs, herein called NNBE(T)s, found in the same dataset. Previous studies have recorded thousands of NNBE(T)s (e.g., Smith et al., 2004; Wu et al., 2011, 2012), while only 5 NNBE(H)s (Rison et al., 2016) and zero NNBE(L)s have been previously reported. We identified and located 15 NNBE(H)s, 18 NNBE(L)s, and 24 NNBE(T)s that satisfied all our location criteria, namely, Δx and Δy horizontal location uncertainties were < 2 km, and the chi-squared goodness-of-fit was < 5.

The determination that NNBE(L)s and NNBE(H)s initiated some -CG flashes was based mainly on three facts:

1. In both the fast antenna data and the Log-RF data, the change from no electrical activity to electromagnetic pulses of each -CG flash began when either an NNBE(L) or an NNBE(H) occurred (e.g., Figs. 3a, 4a, 5a, and 6a). Thus, as the first detectable event, the NNBE(L) or NNBE(H) is apparently the impulsive initiating event of the -CG flash as described by Marshall et al. (2014).
2. After an NNBE(L) or an NNBE(H), the first classic IB pulse (1^{st}CIBP) in the fast antenna data of each -CG flash occurred close in time (averages of 311 and 136 μs, respectively) to the NNBE(L) or NNBE(H) (e.g., Figs. 3b, 4b, 5b, 6b, 11a, and c). This time interval should be the time of the Initial E-Change or IEC defined by Marshall et al. (2014) and is the second stage in the lightning initiation process outlined by Marshall et al. (2014). Note that the measured NNBE(L)/1^{st}CIBP times and NNBE(H)/1^{st}CIBP times were similar to the IEC durations of -CG flashes (Marshall et al., 2014; Chapman et al., 2017), which also is consistent with the identification of NNBE(L)s and NNBE(H)s as initiating events.
3. After an NNBE(L) or an NNBE(H), the first classic IB pulse in the fast antenna data of each -CG flash occurred close in space (300 m on average) to the NNBE(L) or NNBE(H) (e.g., Figs. 3b, 4b, 5b, 6b, 11b, and d). Since the first classic IB pulse is the third stage in the lightning initiation process as outlined by Marshall et al. (2014), one would also expect the first classic IB pulse to be spatially near the initiating event.

For all three types of NNBEs we have provided example plots showing, apparently for the first time, NNBE fast antenna data and coincident data of NNBE VHF power (Figs. 2–6). For each of the three NNBE groups we have presented the following NNBE properties: altitudes (Fig. 7), fast antenna pulse durations and VHF power pulse durations (Fig. 8), range-normalized fast antenna amplitudes (Fig. 9), VHF source powers (Fig. 10), and for NNBE(L)s and NNBE(H)s, separation times and distances between each NNBE and the first classic IB pulse following it (Fig. 11). We also found that the interval between the NNBE(L)s and NNBE(H)s and the first IB pulse (usually a small amplitude, short duration IBP) was characteristically longer than the interpulse intervals during the early part of the IB stage of flash initiation (Fig. 12).

NNBE(H)s and NNBE(L)s occurred at low altitudes, 4.6 to 7.8 km, in keeping with typical initiation altitudes of –CG flashes in mid-latitude storms (e.g., Karunarathna et al., 2017). The NNBE(H)s are single hump events rather than bipolar events; those in our dataset are like the NNBEs discovered and labeled as “more monopolar” by Rison et al. (2016). The NNBE(L)s are low altitude NNBEs that are weaker in power than most NNBE(T)s but have the usual fast antenna bipolar waveform of typical NBEs. NNBE(H)s may simply be weaker versions of NNBE(L)s in which the overshoot peak of the bipolar event is difficult to see, as discussed above and supported by several aspects of the data herein. We speculate that the charge motion of NNBE(L)s and NNBE(H)s may have had a more horizontal orientation than the primarily vertical orientation typically found for positive NBEs. This speculation is worthy of examination in future work. Perhaps related but also needing future study is the intriguing indication in Fig. 13 that most NNBE(H)s may occur above the following IBPs while most NNBE(L)s may occur below them.

Our main conclusions from this study are as follows:

1. As discussed above, the data presented herein indicate that some negative CG flashes are initiated by NNBE(L)s and NNBE(H)s.
2. Visual inspection of the fast antenna and Log-RF data of 868 -CG flashes with locatable IB pulses showed that only 33 flashes (4%) were preceded by an event that can be characterized as an NNBE. Thus, 96% of the -CG flashes investigated probably did not begin with an NNBE. Similarly, Lyu et al. (2019) found that 88% of 26 IC flashes were not initiated by a positive NBE. These findings are in contrast to the statement by Rison et al. (2016) “that all in-cloud lightning discharges are initiated by NBE-type fast positive breakdown.”
3. The NNBEs that initiated -CG flashes, namely NNBE(L)s and NNBE(H)s, were substantially weaker than NNBE(T)s (found herein) that did not initiate lightning flashes. They are also much weaker than previously studied positive NBEs that initiated IC flashes. VHF

powers ranged from 1 to 23 W for NNBE(H)s and from 9 to 1290 W for NNBE(L)s versus 260–7420 W for NNBE(T)s (see Fig. 10) and 93,000–274,000 W for three positive NBEs initiating IC flashes (Rison et al., 2016). Marshall et al. (2019) suggested that -CG flashes are easier to initiate than IC flashes since the IEC charge moments of -CG flashes are much smaller than the charge moments of IC flashes; similarly the much smaller powers of NNBEs initiating -CG flashes versus the positive NBEs initiating IC flashes support the hypothesis that -CG flashes preceded by NNBEs are easier to initiate than IC flashes preceded by positive NBEs.

Acknowledgements

We appreciate the assistance of the sensor site hosts: University of Mississippi Electrical Engineering Department, University of Mississippi Field Station, Jan Murray, Scott and Cherry Watkins, Bill and Crystal MacKenzie, and Martha Mills and the North Delta School. Research data used in this paper are available directly from the corresponding author.

Funding

This study was supported by the USA National Science Foundation (grants AGS-1532038, AGS-1742930).

Declarations of interests

None.

Appendix A

Although the NNBE(H) in Fig. 6 was one of the weakest of the 15 NNBE(H)s both in E_{100km} (−0.10 V/m) and in Log-RF power (4 W), Fig. A1 shows that this NNBE is clearly seen in the E-change data recorded at five sensor sites.

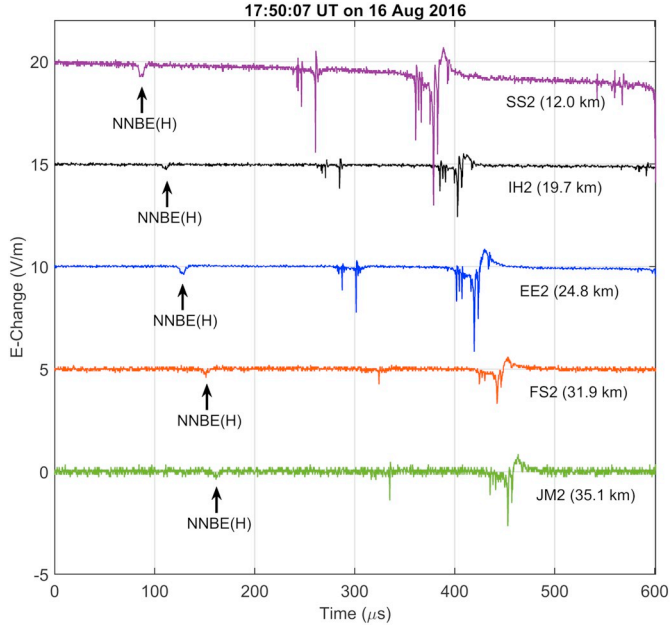

Fig. A1. Plot of the NNBE(H) shown in Fig. 6 at 5 FA sensor sites: JM2, SS2, IH2, FS2, and EE2. The horizontal distance of each sensor from the NNBE(H) is given in parentheses after the site label. From top to bottom the sensor data are progressively farther from the NNBE(H).

References

Azlinda Ahmad, N., Fernando, M., Baharudin, Z.A., Cooray, V., Ahmad, H., Abdul Malek, Z., 2010. Characteristics of narrow bipolar pulses observed in Malaysia. J. Atmos. Solar-Terrestrial Phys. 72, 534–540. https://doi.org/10.1016/j.jastp.2010.02.006.

Balanis, C.A., 2005. Antenna Theory: Analysis and Design, 3rd ed. Wiley-Interscience, New York, NY, USA, pp. 92–95.

Chapman, R., Marshall, T., Karunarathne, S., Stolzenburg, M., 2017. Initial electric field changes of lightning flashes in two thunderstorms. J. Geophys. Res. 122, 3718–3732. https://doi.org/10.1002/2016JD025859.

Jerauld, J., Uman, M.A., Rakov, V.A., Rambo, K.J., Jordan, D.M., Schnetzer, G.H., 2008. Electric and magnetic fields and field derivatives from lightning stepped leaders and first return strokes measured at distances from 100 to 1000 m. J. Geophys. Res. 113, D17111. https://doi.org/10.1029/2008JD010171.

Karunarathna, N., Marshall, T.C., Karunarathne, S., Stolzenburg, M., 2017. Initiation locations of lightning flashes relative to radar reflectivity in four small Florida thunderstorms. J. Geophys. Res. Atmos. 122, 6565–6591. https://doi.org/10.1002/2017JD026566.

Karunarathne, S., Marshall, T.C., Stolzenburg, M., Karunarathna, N., Vickers, L.E., Warner, T.A., Orville, R.E., 2013. Locating initial breakdown pulses using electric field change network. J. Geophys. Res. Atmos. 118, 7129–7141. https://doi.org/10.1002/jgrd.50441.

Karunarathne, S., Marshall, T.C., Stolzenburg, M., Karunarathna, N., 2015. Observations of positive narrow bipolar pulses. J. Geophys. Res. 120, 7128–7143. https://doi.org/10.1002/2015JD023150.

Karunarathne, S., Marshall, T.C., Stolzenburg, M., Karunarathna, N., 2016. Electrostatic field changes and durations of narrow bipolar events. J. Geophys. Res. https://doi.org/10.1002/2016JD024789.

Le Vine, D.M., 1980. Sources of the strongest RF radiation from lightning. J. Geophys. Res. 85, 4091. https://doi.org/10.1029/JC085iC07p04091.

Liu, F., Zhu, B., Lu, G., Qin, Z., Lei, J., Peng, K.-M., Chen, A.B., Huang, A., Cummer, S.A., Chen, M., Ma, M., Lyu, F., Zhou, H., 2018. Observations of blue discharges associated with negative narrow bipolar events in active deep convection. Geophys. Res. Lett. 45, 2842–2851. https://doi.org/10.1002/2017GL076207.

Lyu, F., Cummer, S.A., Qin, Z., Chen, M., 2019. Lightning initiation processes imaged with very high frequency broadband interferometry. J. Geophys. Res. Atmos. https://doi.org/10.1029/2018JD029817. 2018JD029817.

Marshall, T., Stolzenburg, M., Karunarathna, N., Karunarathne, S., 2014. Electromagnetic activity before initial breakdown pulses of lightning. J. Geophys. Res. Atmos. 119, 12,558–12,574. https://doi.org/10.1002/2014JD022155.

Marshall, T., Bandara, S., Karunarathne, N., Karunarathne, S., Kolmasova, I., Siedlecki, R., Stolzenburg, M., 2019. A study of lightning flash initiation prior to the first initial breakdown pulse. Atmos. Res. 217, 10–23. https://doi.org/10.1016/j.atmosres.2018.10.013.

Nag, A., DeCarlo, B.A., Rakov, V.A., 2009. Analysis of microsecond- and submicrosecond-scale electric field pulses produced by cloud and ground lightning discharges. Atmos. Res. 91, 316–325.

Rison, W., Thomas, R.J., Krehbiel, P.R., Hamlin, T., Harlin, J., 1999. A GPS-based three-dimensional lightning mapping system: initial observations in Central New Mexico.

Geophys. Res. Lett. 26, 3573–3576. https://doi.org/10.1029/1999GL010856.
Rison, W., Krehbiel, P.R., Stock, M.G., Edens, H.E., Shao, X.M., Thomas, R.J., Stanley, M.A., Zhang, Y., 2016. Observations of narrow bipolar events reveal how lightning is initiated in thunderstorms. Nat. Commun. 7, 1–12. https://doi.org/10.1038/ncomms10721.
Smith, D.A., Shao, X.M., Holden, D.N., Rhodes, C.T., Brook, M., Krehbiel, P.R., Stanley, M., Rison, W., Thomas, R.J., 1999. A distinct class of isolated intracloud lightning discharges and their associated radio emissions. J. Geophys. Res. Atmos. 104, 4189–4212. https://doi.org/10.1029/1998JD200045.
Smith, D.A., Heavner, M.J., Jacobson, A.R., Shao, X.M., Massey, R.S., Sheldon, R.J., Wiens, K.C., 2004. A method for determining intracloud lightning and ionospheric heights from VLF/LF electric field records. Radio Sci. 39https://doi.org/10.1029/2002RS002790. n/a-n/a.
Stutzman, W.L., Thiele, G.A., 2013. Antenna Theory and Design, 3rd ed. John Wiley & Sons, pp. 113–114.
Uman, M.A., McLain, D.K., Krider, E.P., 1975. The electromagnetic radiation from a finite antenna. Am. J. Phys. 43, 33–38. https://doi.org/10.1119/1.10027.
Weidman, C.D., Krider, E.P., 1979. The radiation field wave forms produced by intracloud lightning discharge processes. J. Geophys. Res. 84, 3159. https://doi.org/10.1029/JC084iC06p03159.
Wescott, E.M., Sentman, D., Osborne, D., Hampton, D., Heavner, M., 1995. Preliminary results from the Sprites 94 Aircraft Campaign: 2. Blue jets. Geophys. Res. Lett. 22, 1209–1212. https://doi.org/10.1029/95GL00582.
Willett, J.C., Bailey, J.C., Krider, E.P., 1989. A class of unusual lightning electric field waveforms with very strong high-frequency radiation. J. Geophys. Res. 94, 16255. https://doi.org/10.1029/JD094iD13p16255.
Wu, T., Dong, W., Zhang, Y., Wang, T., 2011. Comparison of positive and negative compact intracloud discharges. J. Geophys. Res. 116, D03111. https://doi.org/10.1029/2010JD015233.
Wu, T., Dong, W., Zhang, Y., Funaki, T., Yoshida, S., Morimoto, T., Ushio, T., Kawasaki, Z., 2012. Discharge height of lightning narrow bipolar events. J. Geophys. Res. Atmos. 117. https://doi.org/10.1029/2011JD017054.